UNIVERSITÉ LAVAL

Multiplexage par Division Modale pour les Applications à Courte Distance

Thèse

Reza Mirzaei Nejad

Doctorat en Génie Électrique

Philosophiæ doctor (Ph.D.)

Québec, Canada

Résumé

Le multiplexage par division de mode (MDM) a reçu une attention considérable de la part des chercheurs au cours des dernières années. La principale motivation derrière l'utilisation de différents modes de fibre optique est d'augmenter la capacité des réseaux de transport. Les expériences initiales ont montré une grande complexité dans le traitement de signal (DSP) du récepteur. Dans cette thèse, nous étudions la viabilité et les défis de la transmission de données sur des fibres à quelques modes (FMF) pour des systèmes MDM à complexité de DSP réduite. Nos études comprennent à la fois une transmission de données cohérente et non cohérente.

Dans notre première contribution, nous démontrons, pour la première fois, la transmission de données sur 4 canaux dans une nouvelle fibre OAM sans démultiplexage de polarisation optique. Nous utilisons une complexité de DSP réduite: deux jeux d'égaliseurs MIMO (multiple-input multiple-output) 2 × 2 au lieu d'un bloc égaliseur MIMO 4 × 4 complet. Nous proposons un nouveau démultiplexeur de mode permettant de recevoir simultanément deux polarisations d'un mode et de réaliser électriquement un démultiplexage de polarisation dans le récepteur DSP. Nous étudions également la pénalité OSNR due aux imperfections dans le démultiplexeur de mode et nous examinons la vitesse de transmission maximum accessible pour notre système.

Dans notre deuxième contribution, nous étudions les dégradations modales dans les systèmes OAM-MDM, en nous concentrant sur leur effet sur la performance et la complexité du récepteur. Dans notre étude expérimentale, nous discutons pour la première fois de l'impact de deux modes non porteurs de données sur les canaux de données véhiculés par les modes OAM. Deux types différents de fibres OAM sont étudiés. Nous caractérisons notre liaison MDM en utilisant les techniques de mesure du temps de vol et de réponse impulsionnelle. Nous discutons des conclusions des résultats de caractérisation en étudiant l'impact des interactions modales sur la complexité de l'égaliseur du récepteur pour différents scénarios de transmission de données.

Dans le troisième chapitre, nous étudions un nouveau FMF à maintien de polarisation et conduisons deux séries d'expériences de transmission de données cohérentes et de radio sur fibre (RoF). Nous démontrons pour la première fois, la transmission de données sans MIMO sur six et quatre canaux dans les systèmes cohérents et RoF, respectivement. Nous démontrons également, pour la première fois, la transmission de données RoF sur deux polarisations d'un mode dans une FMF. Nous discutons de la dégradation des performances due à la diaphonie dans de tels systèmes. Nous étudions également l'impact de la courbure sur cette fibre dans un contexte de RoF. La propriété de maintien de polarisation de cette fibre sous courbure est étudiée à la fois par des expériences de caractérisation et de transmission de données.

Abstract

Mode division multiplexing (MDM) has received extensive attention by researchers in the last few years. The main motivation behind using different modes of optical fiber is to increase the capacity of transport networks. Initial experiments showed high complexity in DSP of the receiver. In this thesis, we investigate the viability and challenges for data transmission over specially designed few mode fibers (FMF) for MDM systems with reduced DSP. Our studies include both coherent and non-coherent data transmission.

In our first contribution, we demonstrate, for the first time, data transmission over 4 channels in a novel OAM fiber without optical polarization demultiplexing. We use reduced DSP complexity: two sets of 2×2 multiple-input multiple-output (MIMO) equalizers instead of a full 4×4 MIMO equalizer block. We propose a novel mode demultiplexer enabling us to receive two polarizations of a mode simultaneously and conducting polarization demultiplexing electrically in receiver DSP. We also investigate the OSNR penalty due to imperfections in the mode demultiplexer and we examine the maximum reachable baud rate for our system.

In our second contribution, we study the modal impairments in OAM-MDM systems, focusing on their effect on receiver performance and complexity. In our experimental study, for the first time, we discuss the impact of two non-data carrying modes on data channels carried by OAM modes. Two different types of OAM fibers are studied. We characterize our MDM link using time-of-flight and impulse response measurement techniques. We discuss conclusions from characterization results with studies of the impact of modal interactions on receiver equalizer complexity for different data transmission scenarios .

In the third contribution, we study a novel polarization-maintaining FMF and conduct two sets of coherent data transmission and non-coherent radio over fiber (RoF) experiments. We demonstrate for the first time, MIMO –Free data transmission over six and four channels in coherent and RoF systems, respectively. We also demonstrate, for the first time, RoF data transmission over two polarizations of a mode in a FMF. We discuss the performance degradation due to crosstalk in such systems. We also study the impact of bending on this fiber in RoF context. The polarization maintaining property of this fiber under bending is studied both via characterization and data transmission experiments.

Table of Contents

List of Tables

List of Figures

Abbreviations

AWG	Arbitrary Wave Generator
B2B	Back-to-Back
BER	Bit Error Rate
BPG	Bit Pattern Generator
BS	Beam Splitter
CD	Chromatic Dispersion
CP	Cyclic Prefix
CPR	Carrier Phase Recovery
CW	Continuous-Wave
DAC	Digital-to-Analog Converter
DD	Decision Directed
DDO-OFDM	Direct-Detection Optical Orthogonal Frequency-Division Multiplexing
DP	Dual Polarization
DSP	Digital Signal Processing
EDFA	Erbium-Doped Fiber Amplifier
EVM	Error Vector Magnitude
FEC	Forward Error Correction
FFT	Fast Fourier Transform
FIR	Finite Impulse Response
FOR	Frequency Offset Estimation
IFFT	Inverse Fast Fourier Transform
IR	Impulse Response
ISI	Inter-Symbol Interference
LD	Laser Diode

LO	Local Oscillator
LP	Linearly Polarized
LPF	Low-Pass Filter
LW	Line-Width
MDM	Mode Division Multiplexing
M-QAM	M-Ary Quadrature amplitude modulation
MIMO	Multiple-input multiple-output
MMSE	Minimum mean square error
MZM	Mach-Zehnder modulator
NRZ	Non-return-to-zero
OAM	Orbital Angular Momentum
OBPF	Optical band pass filter
OFDM	Orthogonal frequency-division multiplexing
OSA	Optical Spectrum Analyzer
OSNR	Optical signal-to-noise ratio
P/S	Parallel-to-serial
PBC	Polarization beam combiner
PBS	Polarization Beam Splitter
PC	Polarization controller
PD	Photo-Detector
PDM	Polarization-division multiplexing
PMD	Polarization Mode Dispersion
PRBS	Pseudorandom binary sequence
QAM	Quadrature Amplitude Modulation
QPSK	Quadrature phase-shift keying
RF	Radio frequency

RTO	Real-time oscilloscope
S/P	Serial-to-parallel
SDM	Space Division Multiplexing
SE	Spectral efficiency
SMF	Single-mode fiber
TDM	Time-division multiplexing
ToF	Time of Flight
VOA	Variable optical attenuator
WDM	Wavelength-division multiplexing

List of Symbols

m	Modulation order
n	Number of bits per symbol
t_i	Transmitted signal in i^{th} channel
r_i	Received signal in i^{th} channel
τ_i	Differential mode group delay of mode i
D	Number of modes used in system
R_i	Fourier transform of the received signal in i^{th} channel
T_i	Fourier transform of the transmitted signal in i^{th} channel
H_{ij}	Channel transfer function for sending channel i and receiving channel j
u_{ij}	Equalizer output for sending polarization i and receiving polarization j
V_i	Equalizer output for polarization i
w_{ij}	Equalizer filter coefficients for case of sending channel i and receiving channel j
L	Number of taps of equalizer
Δ	Step of convergence for equalization algorithm
ε	Error function in equalization algorithm tap update
P_{ij}	Received power when sending channel i and receiving channel j

To my parents,
Esfandyar and Mah Monir

Acknowledgment

I would like to express my sincere gratitude to my director, Professor Leslie A. Rusch, for all she taught me during my Ph.D. studies. For a project with extensive experimental studies, I faced many challenges but I never felt alone in this way and always had her support and help. I admire the considerable amount of time she spent with me going step by step through different phases of this project. I do appreciate her guidance, kindness and patience throughout my studies during these years.

I would also like to thank Prof. Sophie LaRochelle, member of COPL, who has been involved in this project and helped me wherever possible.

Next, I would like to thank the post docs with who I spent a lot of my time in the laboratory: Dr. Pravin Vaity for invaluable efforts to build the free space optics setup for mode multiplexer and demultiplexer and running the initial experiments with me; Dr. Karen Allahverdyan who committedly came to laboratory with me every single day including weekends. A special thanks to Dr. Lixian Wang who helped me after Karen left our group. His enthusiasm for academic research is admirable. I would also like to thank Farzan Tavakoli who helped me in the last few months of the experiments.

I had the chance to find many good friends at COPL who were part of my life here. I would like to thank Hadi, Siamak, Amin, Hassan, Bahareh, Alessandro, Charles, Gabriel and Omid for the good times we spent together.

Last but not least, I would like to thank my family who always encouraged me to pursue my studies and always supported me during all these long years that I have been in academia.

Foreword

Three chapters of this thesis are based on materials published in conference and journal papers. Most of the contents in these three chapters are the same as the journal papers; however, some modifications are made to the introduction of chapters and some supportive material are added for better coherence. I was the main contributor to these papers

Chapter 3: Reza Mirzaei Nejad, Karen Allahverdyan, Pravin Vaity, Siamak Amiralizadeh, Charles Brunet, Younès Messaddeq, Sophie LaRochelle, and Leslie Ann Rusch, "Mode Division Multiplexing Using Orbital Angular Momentum Modes Over 1.4-km Ring Core Fiber," Journal of Lightwave Technology, vol. 34, no. 18, Sept. 2016.

This paper demonstrates for the first time, data transmission over four channels using OAM modes of order zero and one with reduced DSP complexity. Two sets of 2×2 equalizer blocks were used instead of a full 4×4 MIMO equalizer. We used, for the first time, electrical polarization demultiplexing in OAM-MDM systems. Karen Allahverdyan and Pravin Vaity helped me with the free space optics setup. Siamak Amiralizadeh helped me with optical signal to noise ratio sweeping. Charles Brunet designed the fiber used in the experiment. Younès Messaddeq and Sophie Larochelle gave guidance for fiber design and fabrication. Leslie A. Rusch guided and managed the whole project including fiber design, building the setup and data transmission experiments. I built and ran the data transmission setup; debugged and completed the offline DSP; helped with the finalizing the free space setup and having a clear alignment routine. I wrote the paper and it was revised by the co-authors.

Chapter 4: Reza Mirzaei Nejad, Lixian Wang, Jiachuan Lin, Sophie LaRochelle, and Leslie A. Rusch, "The impact of Modal Impairments on Receiver Complexity in OAM Fibers," Journal of Lightwave Technology, vol. 35, no. 21, Nov. 2017.

This paper discusses the modal impairments observed during OAM fiber characterization and how these impairments affect receiver complexity and the performance of the equalizer block. Lixian Wang helped me with the free space optics setup and fiber characterization. Jiachuan Lin helped me with the data transmission. Sophie LaRochelle advised us on characterization techniques. The project was led by Leslie A. Rusch. I did the experiments and analyzed the results in the discussions section. I chose the characterization techniques required; completed measurements and analyzed results from data transmission. I wrote the paper and it was revised by the co-authors.

Chapter 5: Reza Mirzaei Nejad, Farzan Tavakoli, Lixian Wang, Xun Guan, Sophie LaRochelle, and Leslie A. Rusch, "RoF Data Transmission using Four Linearly Polarized Vector Modes of a Polarization Maintaining Elliptical Ring Core Fiber," submitted to Journal of Lightwave Technology. Lixian Wang, Reza Mirzaei Nejad, Alessandro Corsi, Jiachuan Lin, Younès Messaddeq, Leslie Rusch, and Sophie Larochelle, "Linearly polarized vector modes: enabling MIMO-free mode-division multiplexing," Optics Express, vol. 25, no. 10, pp.11736-11748, May 2017.

For the first paper, Farzan Tavakoli and Lixian Wang helped with building the free space optics setup. Xun Guan provided me with his DSP code for narrowband OFDM transmission and reception. I built and ran the data transmission setup. I also proposed the ideas for performance evaluation in RoF context and investigating the bending characteristic and polarization maintaining properties of the fiber using data transmission results. I wrote the paper and it was revised by the co-authors.

I was the second author of the second paper. I did the data transmission experiment. The sections describing the data transmission setup and the performance evaluation results are extracted from this paper and discussed and compared with the results of first paper of this chapter in the thesis.

Chapter 1

Introduction

1.1. Capacity crunch in optical transport network

The amount of traffic carried by optical transport networks has increased rapidly over the last decades. In the past two decades, and due to new telecom and Datacom services, a growth of around 30 to 60% per year in different geographic regions was observed [1], [2]. New applications, which require higher bandwidth, are being introduced every day. The number of users for different services, from digital media to mobile applications is increasing annually and will require more and more bandwidth in fiber optics backbone networks [3], [4]. In this section, we first review the technologies that have helped to increase the capacity of optical transport networks over the past decades. Next, we discuss the solutions to increase capacity in future networks.

The timeline of bit rate increase in optical transmission systems with different technologies is shown in Fig. 1.1. For over two decades, the bit rate increase was achieved via wavelength-division multiplexed (WDM) optical transmission systems [5]. This was itself mainly accomplished by improvements in optoelectronic device technologies. For

example, by introduction of lasers that could reach GHz frequency stability and optical filters that would let the engineers exploit 50 GHz frequency grids, the capacity was further increased.

After developments in physical technologies leading to better and more sophisticated devices, in the next phase, the telecommunication techniques played a significant role to increase the spectral efficiency by sending more information in the same bandwidth provided by optical devices. In the last decade, we have observed the adoption of many concepts from wireless communications in optical communications. This includes several techniques such as i) higher order modulation formats, i.e., quadrature amplitude modulation (QAM) accompanied with coherent detection instead of simply a non-coherent on-off keying modulation, ii) different digital signal processing (DSP) techniques and also iii) error correction coding [6-9].

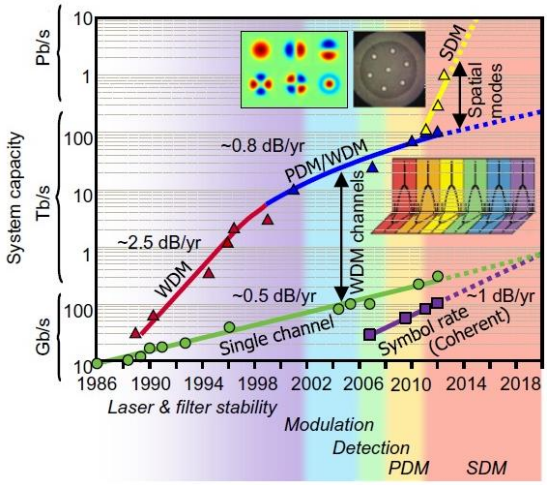

Fig. 1.1. Time line for bit rate increase of optical transmission systems with different technologies [10]

While the single mode optical fiber transmission systems are reaching their capacity limit imposed by the combination of Shannon's information capacity limit and nonlinear fiber effects [11], the demand for higher capacity is still increasing annually. Considering this issue, alternative techniques are required to support the amount of traffic foreseen for future networks.

In Fig. 1.2, all the physical dimensions in an optical fiber that can be used to create orthogonal signal sets for either modulation or multiplexing are illustrated.

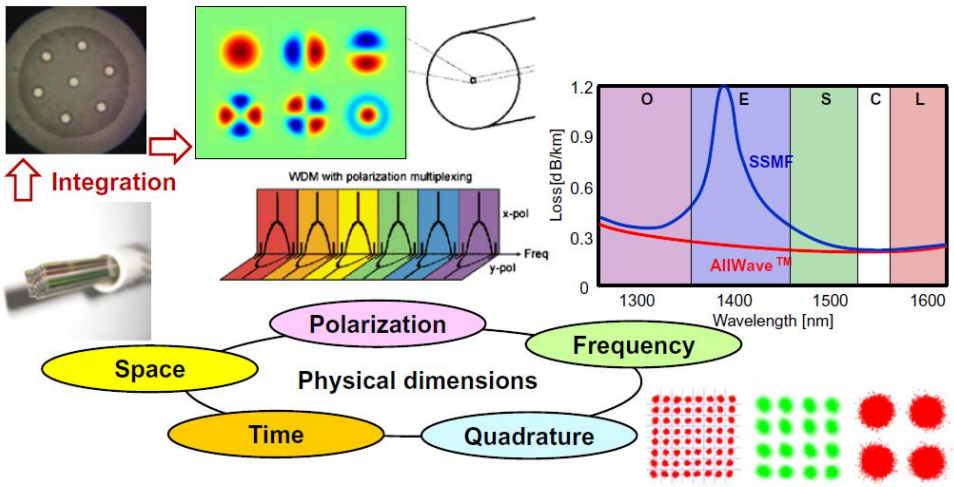

Fig. 1.2. Different physical technologies to create orthogonal signal sets [10]

In what follows, we briefly review them:

I) The quadrature dimension which is the in-phase and quadrature components of the signal, are used to create higher order modulation formats, i.e. quadrature amplitude modulation (*m*QAM) formats where the number of bits per symbol, *n*, is increased by the order of modulation, *m*, following the expression $n = \log_2 m$ bits per symbol. As the modulation order is increased, system performance will be more sensitive to noises and impairments of optical links, resulting in system performance degradation and imposing a restriction to using high spectral efficiency when a certain bit error rate (BER) is required.

II) The frequency dimension is used for multiplexing different data channels to different wavelengths in WDM systems. The capacity is scaled by the number of frequency channels used by the system. However, WDM related impairments, as

well as the available frequency band and the bandwidth of optical components used in the transmission link, limit the arbitrary increase in number of frequency channels.

III) The polarization dimension is used for polarization-division multiplexing (PDM). It can give a two-fold increase in capacity by sending two data streams on two orthogonal polarization states of the fundamental mode propagating in single mode fiber.

IV) The time dimension is used for multiplexing where different time slots are assigned to different channels to create a time division multiplexing (TDM) system. This technique clearly cannot increase the capacity of the network but it can be used as a way to share the same channel between different users.

V) The space dimension uses different modes of fiber as independent data channels to increase the capacity scaled by the number of modes exploited. Since the number of modes supported by fibers can be infinite in theory, there is a huge interest in studying the possibilities of space division multiplexing (SDM) or mode division multiplexing (MDM) as the main candidate for capacity increase in future networks. We will discuss MDM systems in more detail in the next section.

1.2. Mode division multiplexing

In MDM, different modes out of an orthogonal modal basis are chosen as independent data channels. Exploiting more than one mode, and combining the idea of MDM with currently available WDM systems, can significantly increase the capacity of transport networks. The conceptual diagram for the key components in MDM system is shown in Fig. 1.3, where t_i and r_i are the transmitted and received data for i^{th} channel, respectively

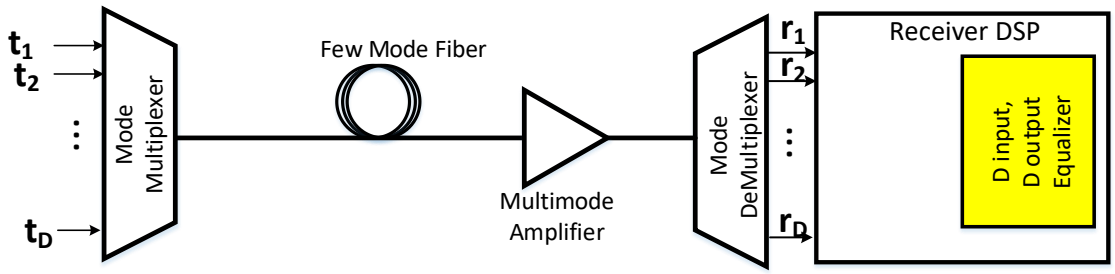

Fig. 1.3. The key components of a MDM transmission system

The key components in MDM systems include modal multiplexer /demultiplexer, few mode fiber (FMF) and multimode amplifiers. For mode (de)multiplexing, different techniques and devices have been used such as phase plates [12], spatial phase modulators [13] or photonic lanterns [14]. New fibers are being developed for MDM systems supporting different number of modes [15]. Research on multimode amplifiers that could amplify the modes supported by the MDM system with the same gain value is another important research area [16] that can lead to a fundamental improvement in reach and capacity of MDM systems.

Although MDM systems can increase the capacity of transport networks, they suffer from modal impairments that can affect the performance or complexity of the receiver. The two main impairments in the linear regime in MDM systems include modal coupling and modal dispersion. With a well-designed fiber, modal coupling, i.e., crosstalk, can still occur in an MDM link due to various reasons such as fiber imperfection, non-ideal mode multiplexer and demultiplexer or mechanical stresses such as bending and twisting. Modal dispersion or differential mode group delay (DMGD) occurs as different modes have different group velocities and therefore, they travel with different speeds in the fiber. If D independent signals are launched at the transmitter on D modes simultaneously, they arrive at the receiver in different times with different group delays (GD), τ_i, i =1, 2, .. D.

DSP in MDM systems is used to compensate the modal impairments. They key block to compensate the modal impairments is the equalizer block. In general, for a system using D channels, an equalizer block with D inputs and D outputs is required. DMGD among different modes can affect the memory depth requirement of equalizers.

Depending on the strength of modal coupling among different modes, MDM systems can be divided to two groups of "*strong*" and "*weak*" mode coupling. In general, the level of modal crosstalk can affect the required dimension of the equalizer block. The equalizer block complexity, for these two groups of systems are different. In next section, we will discuss the structure and complexity of the equalizer block for MDM systems in strong and weak coupling regimes.

1.3. Equalizer complexity in MDM systems

An equalizer block in the receiver DSP of coherent detection systems is responsible for correcting the impairments introduced by the channel and the devices used at the transmitter and receiver side of the system [17]. One important task of equalizer for systems using more than one polarization of one mode is to undo the coupling between different polarization channels. In next sections, we first discuss the structure of equalizer for the current single-mode, commercial PDM systems, and then we discuss the generalization to MDM systems and the ensuing challenges.

1.3.1. Polarization demultiplexing in single mode dual polarization systems

PDM systems use two polarizations of the fundamental mode as two independent data channels. Signals on the two polarization (*X* and *Y)* mix with each other during fiber propagation. The channel interactions can be described in the frequency domain in matrix form as

$$\begin{bmatrix} R_1(\omega) \\ R_2(\omega) \end{bmatrix} = \begin{bmatrix} H_{11}(\omega) & H_{12}(\omega) \\ H_{21}(\omega) & H_{22}(\omega) \end{bmatrix} \begin{bmatrix} T_1(\omega) \\ T_2(\omega) \end{bmatrix} \tag{1.1}$$

where R_1, R_2, T_1 and T_2 are the received and transmitted signals in two polarizations of X and Y, respectively at frequency ω. This is the transfer function, also called the Jones matrix, representation where H_{ij} indicates the channel frequency response when sending polarization i and receiving polarization j. To recover the signal in each of the polarizations, we need an equalizer block that implements the inverse of the channel frequency response.

The equalizer block should receive the two polarization tributaries simultaneously to compensate for the polarization related impairments such as polarization mixing and polarization mode dispersion (PMD). The signals received in two polarizations are equalized using the so-called butterfly equalizer structure shown in Fig. 1.4, where w_{ij} are vectors of the time domain filter taps of the equalizer to recover the desired signal for polarization j from the received signal in polarization i. These taps are the inverse Fourier transform of the frequency response in the Jones matrix, and u_{ij} indicates the equalizer output where the input is from polarization i to recover the data in polarization j.

For short reach applications, where PMD is negligible, it is possible to use a polarization controller on the fiber and undo the polarization mixing optically. By using this method, we do not need the butterfly equalizer structure. However, this method requires constant manual intervention to adjust the paddles of polarization controller to undo the time varying polarization mixing. Modern communications system use more practical electrical polarization demultiplexing in the DSP of receiver. Fig. 1.5 compares these two methods.

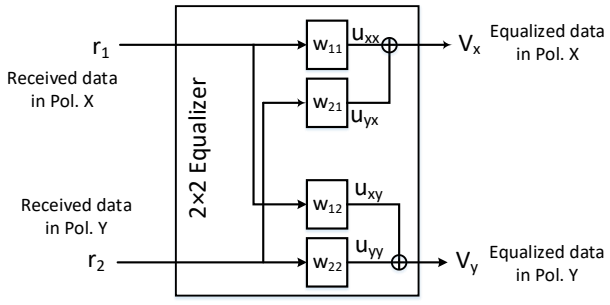

Fig. 1.4. Butterfly Equalizer structure for Polarization demultiplexing

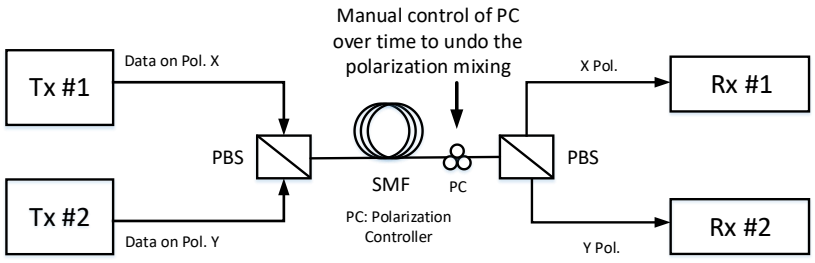

(a)

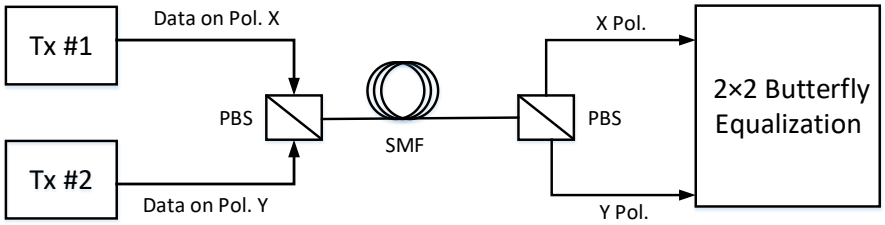

(b)

Fig. 1.5. PDM systems with (a) optical polarization demultiplexing (b) electrical polarization demultiplexing

1.3.2. Equalizer blocks in multi-mode dual polarization systems

For a system that supports transmission of $D/2$ modes in two polarizations carrying D data channels, in general an equalizer block with D inputs and D outputs is required. The task of the equalizer block is to compensate for the modal impairments including modal mixing, i.e. crosstalk, and modal dispersion. In the following, we will discuss the structure of the equalizer block for strong and weak modal coupling regimes.

Mathematically, the transfer function can be described by Eq. (1.2) where T_i and R_i are the transmitted and received signals in the frequency domain for the i^{th} channel, respectively. The channel frequency response is H_{ij} when sending channel (a particular polarization and mode) i and receiving channel j. In the next sections, we discuss the regimes of strong and weak coupling.

$$\begin{bmatrix} T_1(\omega) \\ . \\ . \\ . \\ T_D(\omega) \end{bmatrix} = \begin{bmatrix} H_{11}(\omega) & . & . & . & H_{1D}(\omega) \\ . & . & & & . \\ . & & . & & . \\ . & & & . & . \\ H_{D1}(\omega) & . & . & . & H_{DD}(\omega) \end{bmatrix} \begin{bmatrix} R_1(\omega) \\ . \\ . \\ . \\ R_D(\omega) \end{bmatrix} \quad (1.2)$$

1.3.2.1. Strong mode coupling regime

In this regime, modes of different order fully mix during propagation. All the elements H_{ij} of the channel frequency response matrix are non-zero. To recover the data in each of D channels, a $D\times D$ equalizer block (full MIMO equalizer) should be used to receive and process the data in all D channels simultaneously. The equalizer block should find the inverse of the channel frequency response. As an example, an equalizer block for a 6×6 MDM system is shown in Fig. 1.6 [10]. Here r_i and u_i are the received data and equalized data, for channel i, respectively, and w_{ij} represents the equalizer taps in the time domain to recover the desired signal for channel j from the received signal in channel i.

1.3.2.2. Weak mode coupling regime

In this case, interactions between modes of different order are low; the only strong modal interaction is the polarization mixing. The channel matrix can be regarded as a matrix with zero, or very small, elements that are of the main diagonal and its nearest diagonal on either side. The diagonal 2×2 submatrices represent the polarization mixing within a mode. The transfer function can be described as (1.3)

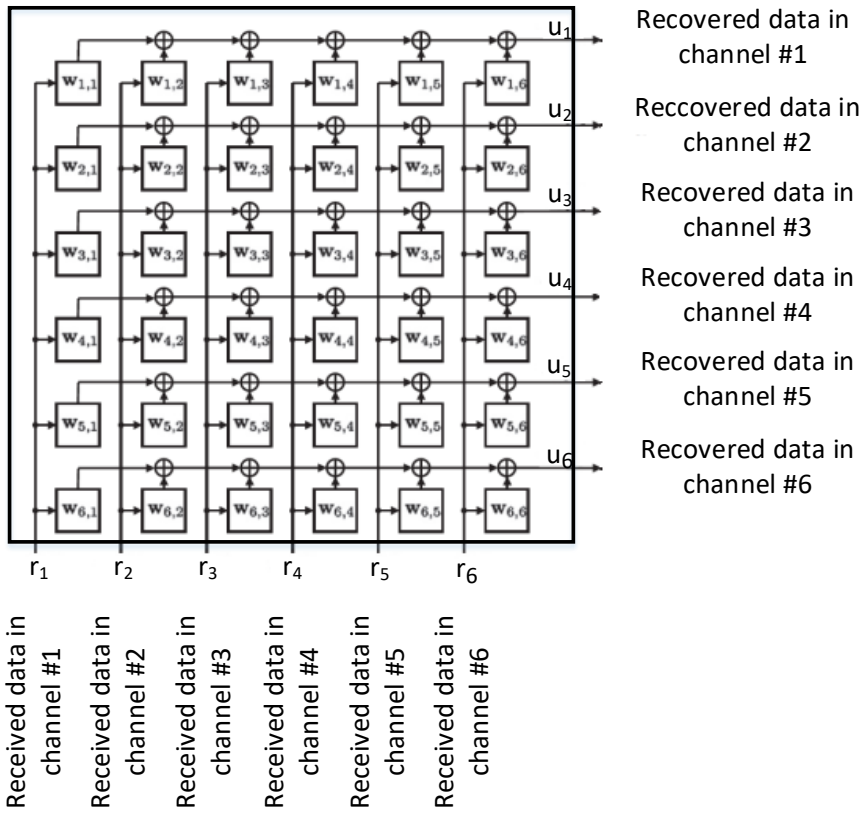

Fig. 1.6. MIMO equalizer structure for a 6×6 MDM system, [10]

$$\begin{bmatrix} \begin{bmatrix} H_{11}(\omega) & H_{12}(\omega) \\ H_{21}(\omega) & H_{22}(\omega) \end{bmatrix} & 0 & .. & 0 \\ . & . & . & . \\ . & . & . & . \\ 0 & . & . & \begin{bmatrix} H_{D-1,D-1}(\omega) & H_{D,D-1}(\omega) \\ H_{D-1,D}(\omega) & H_{D,D}(\omega) \end{bmatrix} \end{bmatrix} \tag{1.3}$$

For sufficiently weak mode coupling, each mode can be detected independently. In practice, this can be achieved by designing specialty fibers with effective indices of

different modes that are sufficiently separated for minimum modal crosstalk. Given two polarizations per mode are used as data transmitting channels, an equalizer block similar to Fig. 1.4 could be used per mode in such systems. Instead of a large equalizer block covering all channels, we will have *D/2* blocks of 2×2 equalizers. These 2×2 equalizers are used to compensate only for polarization mixing within each of the modes. It should be noted that if the polarizations of the modes do not mix with each other, i.e., if they are polarization maintaining, then we simply need *D* equalizers for *D* channels, i.e., a diagonal matrix. The structure of equalizer for such systems is shown in Fig. 1.7.

1.3.2.3. Equalizer complexity comparison between strong and weak mode coupling regimes

As explained in section 1.3.2.1, systems working in the strong coupling regime require full MIMO equalizers. In systems using *D/2* modes and two polarizations per mode, it includes simultaneous reception of *D* channels and MIMO processing with $D \times D$ equalizer blocks, i.e., D^2 equalizers in total. In general, the size of the equalizer block increases with the square of the number of channels. For example, demonstrations using 3 and 15 modes with two polarizations were reported in [18], [19]. For these systems, equalizers with dimension of 6×6 and 30×30 were used, requiring 36 and 900 equalizers in total, respectively. Such equalizer structures can be prohibitively complex for real time realization of receiver DSP in terms of size and power consumptions. The reported demonstrations were using offline DSP processing. Since fabricating fibers for strong coupling regime is less challenging, most of the early MDM transmission demonstrations were in strong coupling regime.

In recent years, researchers are focusing on decreasing the DSP complexity of MDM systems. The main solution is to design fibers and MDM links for separate mode detection, i.e., the weak coupling regime. For systems with separate mode detection, the number of equalizers is linearly related to the number of channels used. Comparing the increase of complexity of equalizers in these two regimes show the advantage and importance of separate mode detection. However, designing fibers and establishing an optical link with low modal mixing is quite challenging.

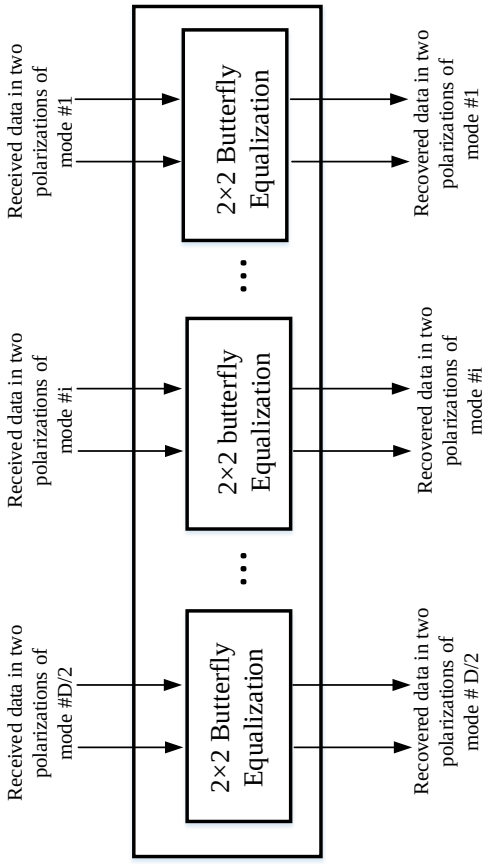

Fig. 1.7. Equalizer block for an MDM system supporting D/2 modes in two polarizations with separate mode detection

1.4. Thesis structure

The motivation behind this project is to study and demonstrate the viability of low complexity MDM systems. The capacity is increased by a multiplicative factor equal to the number of modes, but the complexity is less than the full MIMO processing. For this purpose, different fiber designs are characterized and used in data transmission experiments. In the following, we describe the structure of the thesis.

In chapter 2 we give a brief overview of the electrical digital signal processing used in the characterization and transmission experiments reported in the thesis.

In chapter 3, we discuss data transmission demonstration over an OAM fiber supporting four channels. The experimental setup for data transmission and mode multiplexer and

demultiplexer setup with free space optics components is described in detail. The performance evaluation is presented via BER performance versus optical signal to noise (OSNR) ratio, and BER versus baud rate for high OSNR. The performance penalty due to crosstalk is also discussed. The two main contributions in this chapter include

i) Introducing a polarization diverse mode demultiplexer allowing electrical demultiplexing of the two polarizations of each mode.

ii) Transmitting four channels, for the first time, over an OAM fiber link of length 1.4 km.

In chapter 4, we discuss the modal impairments observed in OAM fibers and how they can affect the receiver complexity and in particular the memory depth of equalizers. Two different type of OAM fibers with different refractive index profiles are studied. The main contributions in this chapter include

i) Channel impulse response measurements for an OAM-MDM system are reported for the first time.

ii) For the first time, the impact of non-data-carrying modes of TE_{01} and TM_{01} on data carrying modes and equalizer memory depth is shown.

iii) The impact of parameters such as differential mode group delay (DMGD) and modal crosstalk on receiver performance and complexity in an OAM-MDM system is discussed based on two characterization techniques (time-of-flight and channel impulse response measurements) and verified via data transmission results.

In chapter 5, data transmission results are reported for another type of fiber designed for separate mode detection. This fiber also benefits from a polarization maintaining property.

Two set of experiments are discussed for coherent detection and radio over fiber (RoF) non-coherent detection. The contributions of this chapter include

i) For the first time, we demonstrated data transmission over six vector mode of a polarization maintaining fiber in a coherent detection scheme. The receiver equalizer structure is even more simplified and instead of a 2×2 equalizer block for processing two polarizations of a mode simultaneously, a single equalizer per polarization of a mode is used.

ii) For the first time, we transmit four radio frequency (RF) signals over four linearly polarized vector modes. The impact of parameters such as RF carrier frequency and modal crosstalk are investigated.

iii) The impact of bending on fiber performance in terms of crosstalk changes and polarization maintaining property are discussed via characterization and data transmission results.

Chapter 2

DSP for MDM systems

2.1. Introduction

In this chapter, we present a very brief review of the structure of the DSP required for the receiver in coherent detection and non-coherent orthogonal frequency division multiplexing (OFDM) systems. We review the blocks for the coherent detection in 2.2. These techniques are used in experiments reported in chapters 3 and 4 and 5. The DSP blocks for non-coherent OFDM systems are reviewed in 2.3. These techniques are used in experiments reported in chapter 5.

2.2. DSP Blocks for Coherent Detection systems

In this section, we review the DSP blocks for coherent detection systems. We start with single-mode, single-polarization systems. We then discuss about the structure of DSP blocks for single-mode, dual-polarization systems.

2.2.1. DSP blocks in single-mode, single-polarization systems

Essential DSP blocks for a conventional coherent detection system is shown in Fig. 2.1 Chromatic dispersion (CD) of the transmission link is compensated by digitally applying

the inverse of the CD transfer function of fiber in the frequency domain [20]. In this thesis, we do not use a block to compensate for CD. All our experiments are with short fibers of

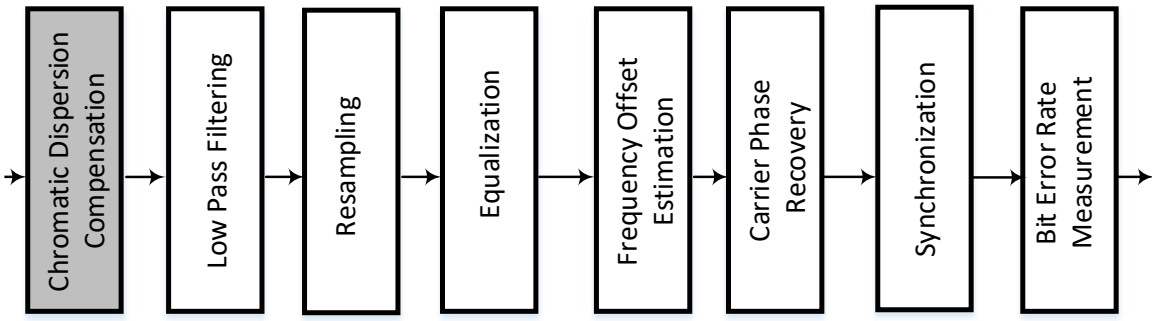

Fig. 2.1. DSP Blocks of a single mode single polarization system

around 1 km. The CD of a short link is negligible and this block is unnecessary for the short reach applications we target.

We low pass filter (LPF) to filter the out-of-band noise. We use a second order super Gaussian filter for this purpose. The bandwidth of the filter is set to 0.7×2× baud rate of the transmitted signal.

The next block is the resampling. The baud rate of the transmitted signal and the sampling rate of the real time oscilloscope (RTO) to capture the data in receiver side are not the same. The resampling block transforms captured data into a vector of received data with an arbitrary number of samples per symbol. This is achieved via interpolation techniques. We used two samples per symbol in our DSP.

Next we have a block for equalization. The equalizer is responsible for correcting the impairments introduced by channel and the devices used in transmitter and receiver side of a coherent detection system. These equalizers are the individual equalizers within the equalizer blocks discussed in chapter 2. The equalizer is realized by a finite impulse response (FIR) filter in the time domain with L taps. The filter coefficients can be found recursively using a steepest descent algorithm. The equalization algorithm could be blind or data aided. In a data-aided approach, the transmitted data is known at the receiver. The two major time domain adaptive algorithms widely used are constant modulus algorithm

(CMA) for blind adaptation and minimum mean square error (MMSE) algorithm for data-aided adaptation [21].

We used blind equalization, i.e., CMA, in all the experiments. The filter coefficients are updated by the expression

$$w^{q,k+1} = w^{q,k} + \Delta \varepsilon_k r_{k-q}^{*} , \quad q = 1,2,...,L \tag{2.1}$$

where $w^{q,k}$ is the complex coefficient of the filter for the q^{th} tap in the k^{th} iteration of convergence, Δ is the step size (set at 10^{-4} in our experiments), ε_k is the error function and r_k is the k^{th} received data sample. Complex conjugate of signal is denoted by *. The error function for CMA for phase shift keying (mPSK) modulation, is defined as

$$\varepsilon_k = u_k(1 - |u_k|^2) \tag{2.2}$$

where u_k is the equalizer output in the k^{th} iteration [22].

The equalizer output, u_k is calculated as

$$u_k = \sum_{i=1}^{L} w_i r_{k-i} \tag{2.4}$$

The next blocks are the frequency offset estimation (FOE) and carrier phase recovery (CPR) blocks. FOE is responsible for compensating the frequency drift between the transmitter and receiver lasers. We used m^{th} power algorithm [23] for FOE which is mainly developed for mPSK modulations. m is the order of modulation, e.g. 4 for QPSK. In our experiments, we always used QPSK modulation, so the fourth power of the received complex signal is calculated. We find the peak in the resulting spectrum. The peak location in the frequency domain gives us the frequency offset between transmitter and receiver lasers.

CPR corrects for the laser phase drift at transmitter and receiver. We used the fourth power algorithm for phase noise correction in our CPR block [23]. This algorithm

calculates the phase drift by finding the angle of the fourth power of the received complex signal, thus removing the data modulation. For better accuracy, this procedure is done by assuming the phase drift is constant over multiple consecutive symbols. We find the angle of the average of fourth power of these symbols and remove it from the received data. We did the averaging over every eight symbols.

The next block is the synchronization block where the cross correlation between the received data and transmitted pseudo random binary sequence (PRBS) is calculated. The location of the peak in the cross correlation allows us to synchronize the received and transmitted data and thus count errors.

The final block is the BER measurement. We first assign the received symbols to the reference symbol in the QPSK constellation at the smallest Euclidean distance. We perform symbol to bit demapping and count errors by comparing the received bit sequence with the transmitted sequence.

2.2.2. DSP blocks in single-mode, dual-polarization systems

PDM systems use two polarizations of the fundamental mode as two independent data channels. The structure of the DSP block of such systems is also that of Fig. 2.1. There are two set of DSP blocks for each tributary at polarizations *X* and *Y* of the fiber, as seen in Fig. 2.2. The main difference with the single polarization system is the equalizer block where the equalizer taps of the two tributaries must be adapted simultaneously and jointly to compensate for the polarization related impairments.

The DSP blocks for PDM systems is shown in Fig. 2.2. The structure of the required 2×2 equalizer block was already discussed in section 1.3.1. Four filters coefficients are updated similar to (2.1), but with a significant difference. Here, the error signal is generated as the difference between the sum of the output of the two constituent equalizers per polarization and the transmitted data on the desired polarization. For example, the error function for the CMA algorithm for *X* polarization, using the same notation as Fig. 1.4., is defined as

$$\varepsilon_k = (u_{xx,k} + u_{yx,k})(1 - |u_{xx,k} + u_{yx,k}|^2) \tag{2.5}$$

where u_{xx} and u_{yx} are the outputs of two equalizers in the butterfly structure in Fig. 1.4 with inputs from received data in polarizations of X and Y used to recover the signal in X polarization; see Fig. 1.4.

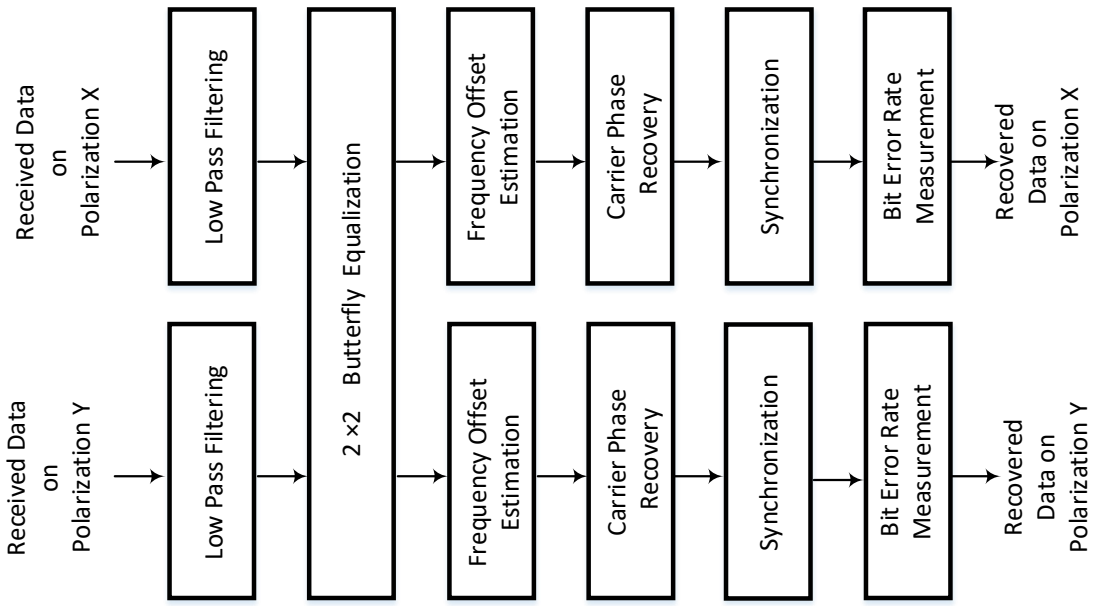

Fig. 2.2. DSP blocks for a single mode dual polarization system

2.3. DSP blocks for non-coherent OFDM systems

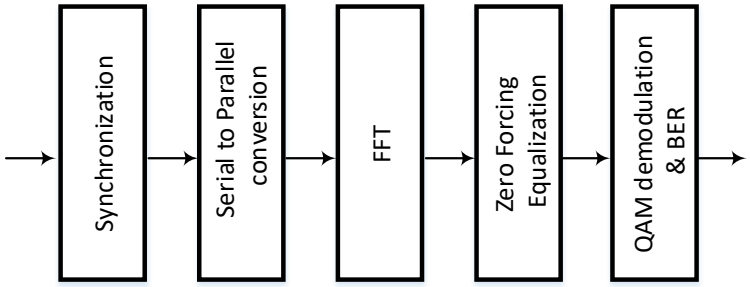

Fig. 2.3. DSP blocks for a non-coherent OFDM systems in (a) transmitter (b) receiver.

In our OFDM data transmission, the OFDM symbols are designed with parameters described in this section. A size 64 fast Fourier transform (FFT) is used, therefore, an OFDM symbol consists of 64 subcarriers in the frequency domain. Of these 64 subcarriers, there are 40 data-carrying subcarriers. Carrier spacing of the baseband OFDM signal is 10MHz. The cyclic prefix ratio of our OFDM symbol is 25%, appended to the beginning of the symbol. In a frame of 20 OFDM symbols, two symbols are used for training to estimate the channel. Subcarriers are modulated with 16 QAM modulation. The DSP blocks at the receiver for non-coherent OFDM systems in single-polarization, single-mode systems is shown in Fig. 2.4.

First, we synchronize the received data and the transmitted data, which is known to receiver. The synchronization block is realized by finding the largest peak in cross-correlation between the received and the transmitted data.

The next block is the serial to parallel formatting, and the removal of the CP. The FFT block converts the received data to the frequency domain.

The equalization block estimates the channel and equalize the received signal in frequency domain. The algorithm used in OFDM systems is the zero forcing algorithm [21], where each subcarrier of OFDM signal is equalized using a one-tap equalizer. We estimate the channel across all the subcarriers by using training symbols and comparing the received symbols with the transmitted ones in the frequency domain. Channel estimation is simply calculated for the two training OFDM symbols as

$$H_i = \frac{R_i}{T_i} \tag{2.6}$$

where R_i and T_i are the received and transmitted symbols on the i^{th} subcarrier; equalization is done over the 40 data-carrying subcarriers. The calculated values for H_i over the two OFDM symbols are averaged together for channel estimation.

The coefficients of the one-tap, zero-forcing equalizers are the inverse of the estimated channel responses. Since the DSP of OFDM is in frequency domain, the output of the equalizer is simply the product of the inverse of the channel and the input data to the equalizer block. Finally, the equalized QAM signal is de-mapped and BER is measured. We do the BER measurement in the same manner as coherent detection explained in section 2.2.1.

The size of the equalizer block for higher number of channels in MDM systems using non-coherent OFDM follows the same rules as those discussed in sections 1.3.2. The strong coupling regime requires a $D \times D$ zero forcing equalizer; in weak coupling regime, the signals can be recovered by 2×2 equalizers per mode. It should be noted that in case of polarization maintaining fibers working under weak coupling regime, the signals can be recovered using D duplicates of the DSP blocks for a single mode single polarization system with one equalizer per channel (Fig. 2.4).

Chapter 3

Mode Division Multiplexing using Orbital Angular Momentum Modes over 1.4 km Ring Core Fiber

Résumé - Les systèmes de multiplexage en division modale (MDM) utilisant des modes de moment angulaire orbital (OAM) peuvent récupérer les données dans différents modes de traitement d'entrée duplex intégral (2D × 2D) - sortie multiple (MIMO). L'un des plus grands défis dans OAM-MDM est l'instabilité du mode suite à la propagation. Auparavant, la transmission de données OAM-MDM sans MIMO avec deux modes sur 1,1 km de fibre vortex a été démontrée lorsque le démultiplexage par polarisation optique était utilisé dans la configuration. Nous démontrons la transmission de données MDM en utilisant deux modes OAM sur 1,4 km d'une fibre à noyau annulaire (RCF) spécialement conçue sans utiliser le traitement MIMO complet ou le démultiplexage à polarisation optique. Nous démontrons l'importance du démultiplexage de polarisation, c'est-à-dire un MIMO minimal de 2×2, montrant la compatibilité de OAM-MDM avec des récepteurs de démultiplexage de polarisation de courant.

Abstract - Mode division multiplexing (MDM) systems using orbital angular momentum (OAM) modes can recover the data in *D* different modes without recourse to full (2*D*×2*D*) multiple input- multiple output (MIMO) processing. One of the biggest challenges in OAM-MDM systems is the modal instability following fiber propagation. Previously, MIMO-free OAM-MDM data transmission with two modes over 1.1 km of vortex fiber was demonstrated where optical polarization demultiplexing was employed in the setup. We demonstrate MDM data transmission using two OAM modes over 1.4 km of a specially designed ring core fiber (RCF) without using full MIMO processing or optical polarization demultiplexing. We demonstrate reception with electrical polarization demultiplexing, i.e.,

minimal 2×2 MIMO, showing the compatibility of OAM-MDM with current polarization demultiplexing receivers.

3.1. Introduction

As discussed in chapter 1, MDM systems have attracted much interest in recent years [24], [25] due to their ability to bypass the capacity limits of single mode systems. We discussed in detail the structure of equalizer block in MDM systems in section 1.4. Most of the demonstrated MDM systems using linear polarization (LP) modes over few mode fibers (FMF) [26] require full MIMO processing in receiver DSP [27]-[29].

Reducing receiver complexity in MDM systems is crucial for feasible real time operation, i.e., for reasonable processing speed and power consumption. Recently, a MIMO-free data transmission was reported over a 100 m graded-index ring core fiber [30]. Only mode groups were multiplexed (not individual modes) and there was no polarization division multiplexing (PDM), greatly reducing capacity. As coupling was negligible between mode groups, and there was no PDM, no MIMO was required. PDM combined with MDM offers highest capacity; but requires a 2×2 equalizer block for polarization demultiplexing for each mode. This is called dual polarization (DP)-MIMO.

Orbital angular momentum modes (OAM) [31] constitute an alternate modal basis for MDM systems. In this chapter, we focus on OAM-MDM data transmission systems. OAM-MDM systems offer the advantage of minimal mode coupling during propagation and thus reduced DSP complexity by eliminating the need for simultaneous detection of all modes and full MIMO processing. However, OAM modes cannot propagate in few mode fibers (FMF) designed for LP modes, but require specially designed fibers. One of the main challenges in OAM-MDM systems is mode instability at the optical fiber output after propagation.

OAM mode propagation was first demonstrated for 20 m and 900 m fibers [32], [33]. Successful MIMO-free OAM-MDM communications over 1.1 km of OAM fiber (called vortex fiber [34]), with simultaneous transmission of 4 channels over two OAM modes (order zero and one), was reported in [35], [36]. While MIMO-free, the transmission

scheme used optical polarization demultiplexing to undo the coupling between the two polarizations in each mode order.

In another experiment [37], successful data recovery without using MIMO processing was reported for OAM MDM data transmission system over 2 and 8 km conventional graded index multimode fiber. As in [30] for LP modes, neither PDM nor individual mode multiplexing was used, rather OAM mode groups (order zero to two) were exploited. Two data channels were constructed by choosing one mode out of degenerate modes inside mode groups of order zero to two (one channel from order zero, the other from order one or two) without polarization diversity.

In this chapter, we demonstrate successful data transmission over 1.4 km of ring core fiber (RCF) in four data channels of two OAM modes in two polarizations. For the first time, to the best of our knowledge, we use a polarization diverse demultiplexing scheme and successful data transmission is achieved without using full MIMO or manual optical polarization demultiplexing. We use electrical polarization demultiplexing in DSP, i.e., 2×2 equalizers for each mode group. We evaluate the BER performance versus OSNR. We examine the case of four channels data transmission and evaluate the OSNR penalty due to increasing the number of channels compared to single channel systems. Furthermore, we discuss the impact of crosstalk in mode demultiplexer and the resulting OSNR penalty.

The remaining sections of this chapter are organized as follows. In section 3.2, we discuss the principal of operation in OAM-MDM systems. In section 3.3, we describe the experimental setup used for data transmission and the details of our free-space, polarization-diverse OAM mux-demultiplexer stages. In section 3.4, we present results for crosstalk measurements in our OAM-MDM link. In section 3.5, we discuss the transmission experiment evaluating our OAM-MDM system performance. In section 3.6, we conclude the chapter.

3.2. Principles of Operation in OAM-MDM Systems

The motivation for using the OAM modal basis is to reduce the complexity of DSP in MDM systems. Complexity can be quantified via the number of equalizers required in

MDM reception. We consider only systems with full capacity where PDM is being combined with MDM, and all modes supported by the transmission system are used as distinct data channels. Therefore, this discussion will not include systems such as [30], [37], [38] where PDM is not used and only mode groups are used for data transmission. In general, for a LP-MDM system with D modes, we need full MIMO with a $2D \times 2D$ equalizer. The number of equalizers required in these LP-MDM systems with full MIMO processing scales with the square of the number of modes. Examples of this increase in complexity include LP-MDM systems (with two polarizations per mode) supporting 3 modes [28] and 15 modes [29], where equalizer blocks of 6×6 and 30×30 were used, respectively.

By using OAM modes, the complexity of DSP can be reduced, as the coupling between different modes can be low enough for separate mode detection. In OAM-MDM systems, the number of equalizers required scales linearly with the number of modes being exploited. As an example, and in our demonstration for a system using two OAM modes of OAM_0 and OAM_1 in two polarizations, supporting 4 data channels, two blocks of 2×2 equalizers (for polarization demultiplexing) are required instead of a 4×4 equalizer block.

We transmit simultaneously four data channels over two OAM modes. The order zero mode, the fundamental mode, is denoted by OAM_{0R} and OAM_{0L} where R and L denote right and left circular polarization, respectively. The order one OAM modes are denoted by OAM_{+1} and OAM_{-1}. The interactions between the two mode groups of order zero and one are reduced to a minimum level by using specialty designed fibers for OAM modes propagation. The two polarizations of each of the two modes (zero and one) are degenerate leading to intra-mode coupling during propagation, i.e., OAM_{0L} couples with OAM_{0R}, and OAM_{+1} couples with OAM_{-1}. Hence, while MIMO processing of 4×4 equalizer can be avoided, polarization demultiplexing on each mode group is required for successful data recovery in such systems.

Demultiplexing in [35], [36] used optical polarization demultiplexing using polarization controllers to separate the two polarizations of each mode rather than electronic separation. The demultiplexer setup was thus sequentially optimized for detection of each channel as they were captured; one polarization of one mode could be detected at a time at the

demultiplexer output. We use a demultiplexing scheme allowing simultaneous detection of two polarizations in each mode group. It enables us to employ electrical polarization demultiplexing in DSP instead of optical polarization demultiplexing (i.e., manipulation of a polarization controller). This is the technique used in all commercial polarization multiplexing systems.

We present results for the transmission of dual polarization quadrature phase shift keying (QPSK) data up to 32 Gbaud on each of 4 channels, for a total rate of 256 Gbps. Without recourse to full MIMO processing, and using conventional DSP for dual polarization single mode coherent detection systems (standard 2×2 MIMO used in single mode fiber systems), we report bit error rate (BER) values below the forward error correction (FEC) threshold for each of the four OAM channels.

3.3. Experimental Setup

Our OAM-MDM link is comprised of three building blocks for mode generation, propagation and reception: a mode multiplexer (mux), a mode demultiplexer (demultiplexer) and specially designed ring core fiber (RCF) for OAM transmission. We first describe test equipment used for signal generation and data capture, followed by a description of the mux, demultiplexer and fiber.

3.3.1. Signal Generation and Reception

We used an SHF 12103A bit pattern generator (BPG) with two pseudo random binary sequences (PRBS) of length 2^{15}-1 and 2^{20}-1 to generate a single polarization non-return-to-zero (NRZ) QPSK signal with an SHF46213D IQ modulator. The transmitter laser has a linewidth of 100 kHz and is set to 1550 nm with output power of 16 dBm. After the modulator, the signal is amplified and then sent to the OAM MDM link. At the receiver side, a single coherent receiver is used. The coherent receiver is connected to the appropriate output port of the OAM-MDM link for the OAM mode to be detected. The OSNR is varied by the use of an attenuator after the Demultiplexer. The polarization

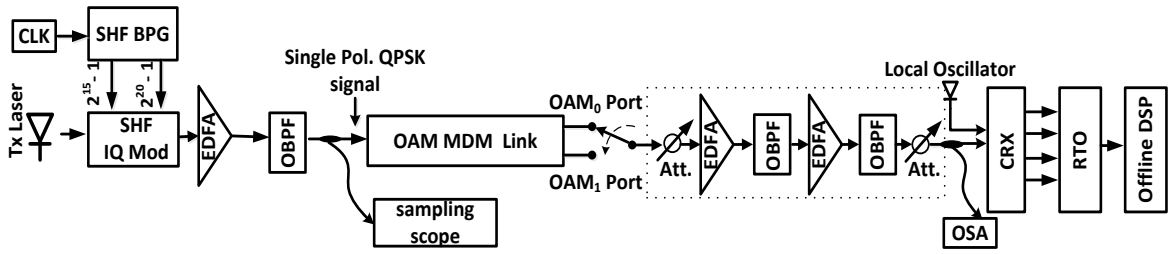

Fig. 3.1. OAM-MDM data transmission setup

diverse signal in the selected mode is directed to a Picometrix coherent receiver with bandwidth of 22 GHz. The power input to the coherent receiver is fixed at -5 dBm. The local oscillator has a linewidth of 10 kHz and has output power of 13 dBm. The output electrical signals from the coherent receiver are captured by a Keysight real-time oscilloscope (RTO) with 30 GHz analog bandwidth capturing data at 80 Gsample/s. We use offline processing to apply conventional DSP for dual polarization single mode coherent detection systems to recover the signals in two polarizations of the mode being detected. No 4×4 MIMO processing is used in our four channel system.

3.3.2. Free space mode multiplexer-demultiplexer stages

The setup for our free space mux-demultiplexer stages is shown in Fig. 3.2(a). In the mode multiplexer stage, the incoming, modulated single polarization signal is first amplified using a high power EDFA with output power of ~23 dBm. The modulated signal is then split into four branches with different delays; the decorrelated replicas of the main data stream are labeled A, B, C and D. The signals in paths A and B are projected on a polarization sensitive spatial light modulator (SLM1) with average permitted power of incident light less than 13dBm. SLM1 is programmed with two separate spiral phase patterns, illustrated in Fig. 3.2(b), to generate OAM_{+1} for path A and OAM_{-1} for path B. A half wave plate (HWP1) rotates the polarization of OAM_{+1} by 90º, i.e., orthogonal to that of OAM_{-1}. The two $OAM_{\pm1}$ modes are then combined using a polarizing beam splitter (PBS1). Paths C and D of OAM_0 (fundamental mode) are combined using a polarization beam combiner (PBC) and finally multiplexed with $OAM_{\pm1}$ at beam splitter BS1. Before

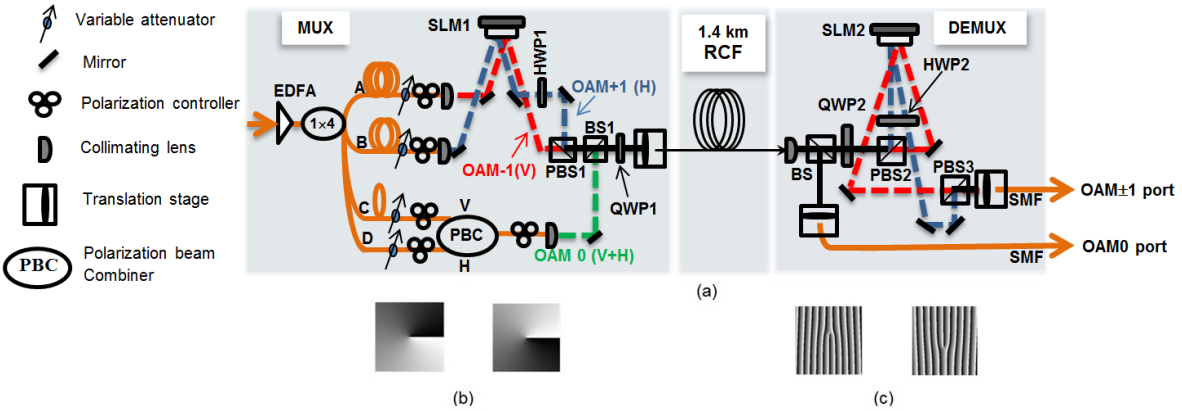

Fig. 3.2. (a) Setup for free-space OAM mux and demultiplexer stages, (b) spiral phase patterns for OAM±1 at SLM of mux stage, (c) blazed forked gratings for OAM±1 at SLM of demultiplexer stage

coupling into the fiber, the multiplexed signal passes through a quarter-wave plate (QWP1) to change the polarization of signals from linear to circular. The multiplexed signal is then coupled into the RCF, described in the next section, using a six-axis translation stage for fiber alignment.

In our polarization diverse mode demultiplexer, we convert a PDM OAM mode to a PDM fundamental mode; all other modes are simultaneously mapped to other OAM modes. Subsequently, the light is coupled to single mode fiber that strips off all but the fundamental mode. The idea of mapping from spatial modes to single mode fibers at the demultiplexer stage was already exploited in MDM systems [37], [38], where pure mode division multiplexing without polarization division multiplexing was used. The mode demultiplexer stage of Fig. 3.2(a) splits the fiber output via BS2 into two different paths, one for OAM_0 mode detection and one for $OAM_{\pm1}$ mode detection. In the OAM_0 path, we couple the signal from free space into a single mode fiber (SMF), using the SMF as a mode stripper for OAM±1; as SMF only supports propagation of OAM_0, $OAM_{\pm1}$ will not couple or propagate in SMF. The output of this port, i.e., the SMF output, nominally only includes data transmitted on the OAM_0 mode group in two polarizations. In reality, the non-zero demultiplexer crosstalk leads to small residual $OAM_{\pm1}$ signals.

For the $OAM_{\pm1}$ path, we must use a polarization sensitive SLM (vertical polarization required) for mode conversion. QWP2 converts the polarization of the received signal from

circular to linear. Vertical and horizontal polarizations are separated using PBS2. The vertical polarization is routed to one section of the SLM. In the horizontal polarization path, a half wave plate (HWP2) assures that a second section of the polarization sensitive SLM2 again receives a vertical polarization. We program SLM2 with two separate blazed forked gratings, illustrated in Fig. 3.2(c), to select OAM_{+1} in one path, and OAM_{-1} in the alternate path. The blazed grating leads the $OAM_{\pm1}$ modes being converted to OAM_0, each with vertical polarization. The alternate path coming through HWP2, passes a second time through that component to be rotated back to horizontal polarization. The idea of using a HWP to rotate the polarization of a beam directed to and reflected from an SLM was also shown in [38]; however, polarization diversity was not used there. The two $OAM_{\pm1}$ modes, newly converted by SLM2 to the fundamental mode, are combined using PBS3. This forms the polarization diverse receiver for $OAM_{\pm1}$.

Finally, the polarization multiplexed signal is coupled into SMF to strip off any residual unwanted OAM_0 signals present. The SMF output at the OAM_1 port is nominally only data from the $OAM_{\pm1}$ modes, now on two polarization states of SMF. After initial free-space mode multiplexer and demultiplexer setup alignment, no further manual intervention (e.g., tuning of polarization) is required in our setup, demonstrating the robustness of OAM-MDM data transmissions.

This demultiplexer scheme can be also used for higher order OAM modes with some modification. For OAM modes of order $|N|\geq2$, there are four data channels in the OAM mode group (an OAM order). A polarization diverse demultiplexer is required for right (R) and left (L) polarizations of each OAM mode (e.g., one for $OAM_{+N}^{R,L}$ and $OAM_{-N}^{R,L}$ modes). We would place a beam splitter after QWP2 and duplicate the paths to SLM. Four surfaces would be programmed on the SLM, two for order $+N$ and $-N$. One SLM surface would be used for one polarization of each of $\pm N$ modes.

3.3.3. Ring Core Fiber

Our OAM fiber is a step-index ring-core fiber supporting OAM_0 and $OAM_{\pm1}$ modes at 1550 nm. The cross section of the fiber is shown in Fig. 3.3(a). The inner radius (a) of the

ring-core is 0.97 µm, and the outer radius (*b*) is 2.78 µm, for a ratio *a*/*b* of 0.35. The cladding has a standard 125 µm diameter. Designed and measured index profiles of fiber are shown in Fig. 3.3(b). The cladding and the center part of the fiber are made of SiO_2, while the ring-core is doped to achieve a refractive index contrast of 0.03 at 1550 nm. This refractive index contrast is sufficiently low to avoid spin-orbit coupling effects that are inherent to thin high-contrast ring-core fibers [39], whereas keeping the fiber fabrication process manageable. These characteristics allow a good effective index separation between the supported modes, preventing the OAM modes to easily couple to LP modes.

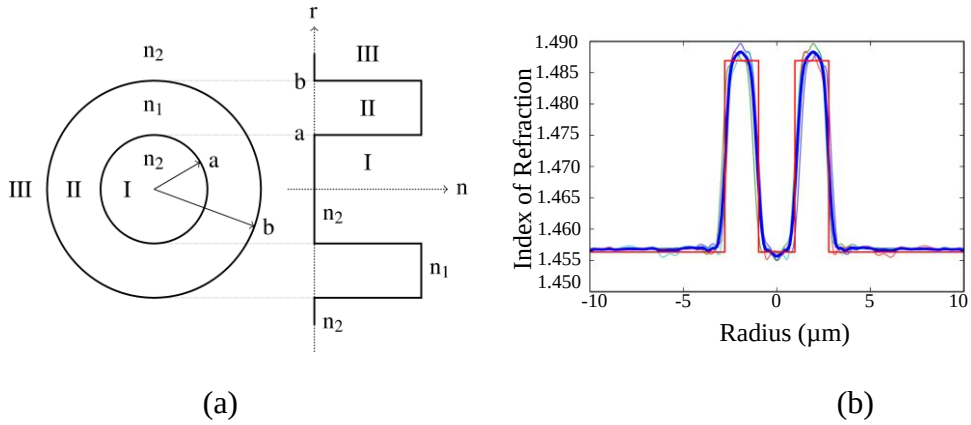

(a) (b)

Fig. 3.3. (a) Cross section of RCF fiber, (b) Designed (red) and measured index profile (blue: averaged, others: x- and y-scan on both directions)

In coupling the free-space, multiplexed $OAM_{\pm1}$ beam into the RCF fiber, the beam intensity ring should perfectly match with the 1.81 µm ring of the RCF fiber core. Misalignment leads to the fundamental mode being excited with $OAM_{\pm1}$ mode, creating crosstalk at the multiplexer stage. The translation stages used to couple the OAM beam into fiber can have their positions vary by as much as a micrometer due to slight (one or two degree Celsius) temperature changes. This can significantly reduce the purity of the excited $OAM_{\pm1}$ modes. Thermo-insulation of translation stages was found highly effective in minimizing this effect in our experiments.

3.4. Crosstalk Measurement

We used power measurements to optimize the manual alignment of our free space OAM mux-demultiplexer stages, and to quantify the crosstalk between the modes. The crosstalk can arise from multiplexing, propagation or demultiplexing. It was monitored and minimized by adjusting free-space beam alignment in mux-demultiplexer stages. In an MDM system low crosstalk is highly desirable, as it results into lower performance penalties. To calculate the crosstalk, we measured the power of the demultiplexer stage output port for a specific mode when 1) transmitting only that mode, and 2) sending the other mode. The ratio between the measured powers indicates coupling from the other mode due to propagation, multiplexing and demultiplexing:

$$\text{Crosstalk on OAM}_i \text{ (dB)} : 10\log\left(\frac{P_{|i-1|}}{P_i}\right), i = 0,1 \tag{3.1}$$

where $P_{|i-1|}$ and P_i are the received powers at demultiplexer output port *i*, for the cases of transmitting OAM modes of order $|i-1|$ and *i* in the RCF fiber, respectively. For the results reported here, we could reach crosstalk levels reported in Table 1. For RCF fiber supporting two OAM modes, the 1.4 km fiber span was the longest fabricated fiber available for data transmission. The mode coupling will increase with fiber length [35]. Data transmission over longer lengths can be investigated in future as longer RCF fiber becomes available.

Table 3.1. Crosstalk measurement for each mode group

Crosstalk on OAM_1 : -10.5 dB	***Crosstalk on OAM_0 : -10.6 dB***
$OAM_{0L} \rightarrow OAM_1$: -13.5 dB	$OAM_{-1} \rightarrow OAM_0$: -13.6 dB
$OAM_{0R} \rightarrow OAM_1$: -13.5 dB	$OAM_{+1} \rightarrow OAM0$: -13.6 dB

3.5. Transmission Experiment

After optimizing the manual alignment of our free space mode multiplexer and demultiplexer stages for minimum crosstalk between modes, we transmitted data and evaluated the performance of our OAM-MDM system. The bit error rate (BER) values are evaluated over 10^6 samples of transmitted data in each data channel during one capture of a PRBS. We did the BER versus OSNR measurement a few times over different days to ensure that our MDM data transmission experiment is repeatable. We focused on minimum achievable BER and the required OSNR to reach the FEC threshold of 3.8×10^{-3}. For these two quantities, there was less than 5% variation over the course of our experiments. This variation could be due to the ±0.1 dB changes in crosstalk levels between channels in the mode multiplexer and demultiplexer alignment on different days.

In Fig. 3.4, BER versus optical signal to noise ratio (OSNR) at baud rate of 16 Gbaud is depicted. As can be observed, for the case of four channels data transmission, we have BER

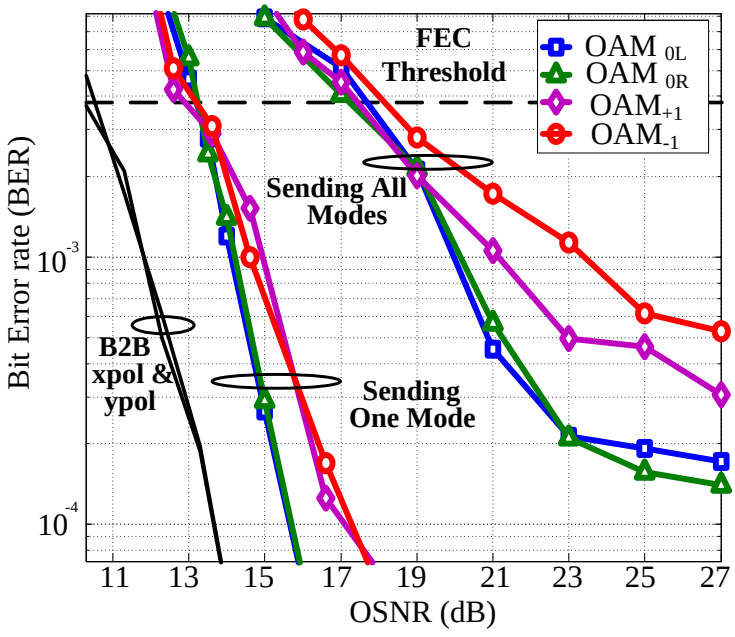

Fig. 3.4. BER vs. OSNR for all four data channel

below the forward error correction (FEC) threshold of 3.8×10^{-3} down to an OSNR of 18 dB. By comparing the cases where a single channel was launched as opposed to all

channels being transmitted, we observe an OSNR penalty of 5 dB at the FEC threshold for switching from single mode to two modes in our OAM-MDM system. This penalty is mostly due to the crosstalk between modes.

In Fig. 3.5, we examine the effect of misalignment in the free-space setup on system performance. We intentionally misalign the SLM in the demultiplexer stage resulting in imperfect mode conversion. Depending on the level of misalignment, we can have different levels of crosstalk from OAM_0 on OAM_1 mode. In Fig. 3.5, we have plotted the OSNR penalty to reach BER of 3.8×10^{-3} as a function of measured crosstalk levels due to the misalignment. The curves are plotted for the case of sending all channels and detecting $OAM_{\pm1}$ modes. As can be observed, small misalignments resulting in low crosstalk increase will be tolerated, whereas an imperfect mode conversion leading to crosstalk values greater than -9 dB will result into dramatic OSNR penalty increase. This is helpful for the study and development of future integrated OAM mux-demultiplexer stages. In particular, the results of this figure highlight the importance and sensitivity of system performance to imperfect mode conversion in demultiplexing.

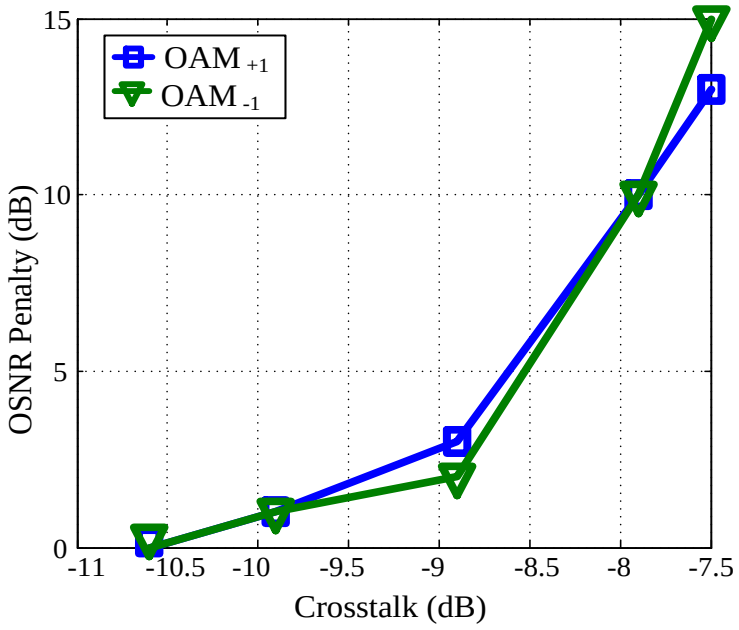

Fig. 3.5. OSNR penalty vs. crosstalk from OAM0 on OAM1 mode group

In Fig. 3.6, we swept the baud rate from 16 to 32 Gbaud at OSNR of ~ 28 dB and reported

BER versus baud rate results. An inset shows typical constellations of the recovered signals at 32 Gbaud. We could reach BER values below the FEC threshold for all four channels for baud rates up to 32Gbaud. It establishes the viability and robustness of OAM mode division multiplexing with reduced DSP (only DP-MIMO) after propagation in 1.4 km of RCF fiber.

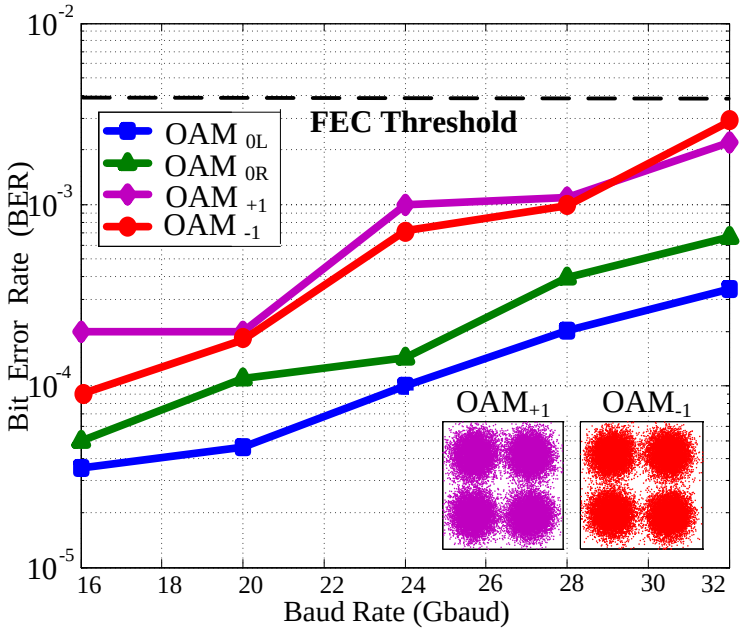

Fig. 3.6. BER vs. baud rate for all four data channels

Baud rate per channel was limited by equipment availability (the coherent receiver has bandwidth of ~22 GHz).

3.6. Conclusions

We have demonstrated for the first time, OAM-MDM with electrical polarization demultiplexing using minimal 2×2 MIMO. We recovered four channels OAM-MDM over 1.4 km of RCF fiber. Taking advantage of our OAM fiber and our polarization diverse OAM mux-demultiplexer scheme, we simultaneously transmitted four channels on two polarizations of two OAM modes, and recovered each mode separately. This was possible due to crosstalk of less than -10.5 dB per mode in our OAM-MDM system. Switching from single mode to two modes data transmission imposes 5 dB OSNR penalty on our system. Data transmission with bit rates up to 4×64 Gbps QPSK was achieved with BER values

below the FEC threshold. No optical control of polarization was used; reception used electrical polarization demultiplexing, showing OAM-MDM is compatible with current polarization demultiplexing receivers.

Chapter 4

The Impact of Modal Interactions on Receiver Complexity in OAM Fibers

Résumé - Nous étudions expérimentalement les interactions modales dans des liaisons de multiplexage par division de mode (MDM) supportant des modes de moment angulaire orbital (OAM) d'ordre zéro et un. Nous utilisons des mesures de temps de vol et de réponse impulsionnelle de canal pour caractériser notre liaison OAM-MDM et quantifier les dégradations modales. Nous examinons deux fibres OAM avec des profils d'indices différents et des retards de groupe de modes différentiels (DMGD) entre les modes vectoriels supportés. Les expériences de transmission de données évaluent l'impact des dégradations modales sur la complexité du traitement du signal numérique et sur le taux d'erreurs binaires réalisable pour la liaison OAM-MDM. Nous discutons en particulier des exigences de profondeur de mémoire pour les égaliseurs dans les schémas de détection en mode séparé, et comment la profondeur de la mémoire varie avec les paramètres liés au DMGD ainsi qu'avec le niveau de diaphonie.

Abstract - We experimentally study the modal interactions in mode division multiplexing (MDM) links supporting orbital angular momentum (OAM) modes of order zero and one. We use time of flight and channel impulse response measurements to characterize our OAM-MDM link and quantify modal impairments. We examine two OAM fibers with different index profiles and differential mode group delays (DMGD) between supported vector modes. Data transmission experiments probe the impact of modal impairments on digital signal processing complexity and achievable bit error rate for OAM-MDM link. We discuss in particular memory depth requirements for equalizers in separate mode detection schemes, and how memory depth varies with DMGD metrics as well as crosstalk level.

4.1. Introduction

Two different modal bases, linearly polarized (LP) modes and orbital angular momentum (OAM) modes are studied for mode division multiplexing by different research groups worldwide [40-46].

Consider two receiver solutions for a *D/2* mode, 2 polarizations per mode MDM system: 1) a monolithic receiver with *D* inputs that are all time synchronized, captured simultaneously and with data processed as one unit, and 2) *D/2* standard receivers, with one receiver per mode and no synchronization or integration between them, with data processed independently. Most demonstrated LP-MDM systems use the monolithic receiver with full MIMO with *D*×*D* equalizers [47], [48].

Several research groups have worked to reduce the dimensionality of MIMO equalizers. The use of separate equalizer blocks for each mode group instead of full MIMO equalizer was investigated for LP modes in [49], [50]. Six modes, each with two polarizations, in four mode groups were detected via four independent detectors with 2×2 or 4×4 equalizer blocks; The use of two independent, uncoordinated receivers for two modes (LP_{01} and LP_{11e}) in [51] led to low dimension (2×2) MIMO equalizer (covering polarization demultiplexing per mode). A polarization maintaining fiber supporting six spatial channels required no MIMO and used six separate receivers, one per channel [52].

OAM fibers were introduced and designed for separate mode detection with low modal coupling [53], [54]. In OAM-MDM systems, our demonstration, discussed in chapter 3, with 4 channels using modes of order zero and one used 2×2 MIMO equalizer for polarization demultiplexing per mode [55]. Another OAM demonstration with 12 channels using mode of order ±5,±6,±7 used only optical polarization demultiplexing to recover the data on each mode [56].

Reducing the MIMO dimensionality results in reducing the DSP burden. The complexity of MIMO processing, however, is governed not only by the number of equalizers (i.e., dimensionality), but also by the memory depth (number of taps) per equalizer. Two linear propagation impairments in MDM systems are related to equalizer block complexity: differential mode group delay (DMGD) and channel crosstalk [57], [58]. We examine the

relationship between modal interactions and DMGD among different propagating modes and OAM-MDM DSP complexity in separate mode detection schemes.

We focus on systems supporting OAM_0, i.e., fundamental mode, in two polarizations, and $OAM_{\pm1}$ mode. We examine two OAM fibers experimentally: a ring core fiber (RCF) [59] and an inverse parabolic graded index fiber (IPGIF) [60]. Each supports OAM_0 and $OAM_{\pm1}$ modes for distances near to one kilometer. HE_{11} and HE_{21} vector modes carry the data channels in these systems; TE_{01} and TM_{01} modes also propagate in OAM-MDM link, but as parasitic modes, i.e., non-data-carrying modes. We will experimentally investigate the impact of modal interactions among data carrying HE_{11} and HE_{21} modes and their interaction with TE_{01}/TM_{01} modes on receiver bit error rate (BER) performance and equalizers required memory depth requirement. The dissimilar refractive index profiles in these fibers lead to different DMGD among vector modes of HE_{11}, HE_{21}, TE_{01} and TM_{01}. In two characterization experiments, we examine time of flight (ToF) and impulse responses (IR) for both 1.47 km RCF and 1.1 km IPGIF fibers. We show the interactions among TE_{01}/TM_{01} and HE_{21} and how it affects the equalizer memory length. As further validation of our hypothesis, we examine another length (450 m) of RCF fiber. Only by examining all these results together can we quantify the impact of parasitic modes on equalizer block complexity.

This chapter is organized as follows. In section 4.2, we discuss the modal interactions in OAM-MDM systems. In section 4.3, we characterize each fiber via ToF and IR measurements. Next, we transmit data and evaluate receiver performance. In section 3.4, we report data transmission results. In section 4.5, we discuss the impact of the modal interactions on required OAM-MDM equalizer memory depth by contrasting the two OAM fibers. In section 4.6, we present the conclusion of the chapter.

4.2. Modal Impairments in OAM-MDM systems

OAM modes are formed from an orthogonal combination of even and odd *HE* and *EH* fiber vector modes and denoted in the paired subscript by its order or topological charge *l* and the number *m* of concentric rings in the intensity profile. We use a superscript "+" for right

circular polarization and "–" for left circular polarization. For OAM modes of order $|l| \geq 2$, there are four OAM modes formed by *HE* and *EH* vector modes

$$OAM_{\pm|l|,m}^{\pm} = HE_{|l|+1,m}^{even} \pm i\, HE_{|l|+1,m}^{odd} \tag{4.1}$$

$$OAM_{\pm|l|,\mathrm{m}}^{\mp} = EH_{|l|-1,\mathrm{m}}^{even} \pm i\, EH_{|l|\text{-}1,m}^{odd} \tag{4.2}$$

The OAM wave-front rotation is in the same orientation as the circular polarization of the *HE* vector modes, and in the opposing orientation for *EH* vector modes. For OAM modes of order one, exceptionally, there are only two OAM modes, OAM_{+1} with right circular polarization (OAM_{+1}^{+}) and OAM_{-1} with left circular polarization (OAM_{-1}^{-}):

$$OAM_{\pm 1}^{\pm} = HE_{21}^{even} \pm i\, HE_{21}^{odd} \tag{4.3}$$

The two other OAM modes of order one, formed by TE_{01} and TM_{01}, are known to be unstable [61]

$$OAM_{\pm 1}^{\mp} = TE_{01} \pm i\, TM_{01} \tag{4.4}$$

The unequal effective indices of TE_{01} and TM_{01} modes cause them to travel at different speeds, leading to walk-off and instability.

OAM mode of order zero, i.e. without any topological charge, is equivalent to fundamental mode carried by HE_{11} mode. In the previous chapter we used notations of $OAM_{0,R}$ and $OAM_{0,L}$ for fundamental mode in right and left polarizations, respectively. Here, and for consistency with the notations in 4.3 and 4.4, we use notations of OAM_{0}^{+} and OAM_{0}^{-} which signify fundamental mode with right and left circular polarization, respectively.

Throughout our discussions in characterization and data transmission, when we discuss H_{11} mode, this refers directly to data bearing $OAM0^{\pm}$ modes. When we discuss H_{21} mode, this refers directly to the data bearing $OAM_{\pm 1}$ modes.

In this chapter, we focus on fibers supporting OAM modes of order zero and one and their constituent vector modes HE_{11}, HE_{21}, TE_{01} and TM_{01}. Contrary to LP-MDM systems

where all vector modes are exploited as data channels, in first order OAM-MDM systems the TE_{01} and TM_{01} modes are neither intentionally excited at transmission, nor detected at reception. These modes can, however, be unintentionally excited and become parasitic modes.

Fig. 4.1, illustrates propagation modes in a fiber in an OAM system. $OAM_0^{\pm}$ and $OAM_{\pm1}$ modes are injected into the fiber via a mode multiplexer. These modes should excite primary vector modes HE_{11} and HE_{21}. Due to undesired crosstalk, there may be leakage

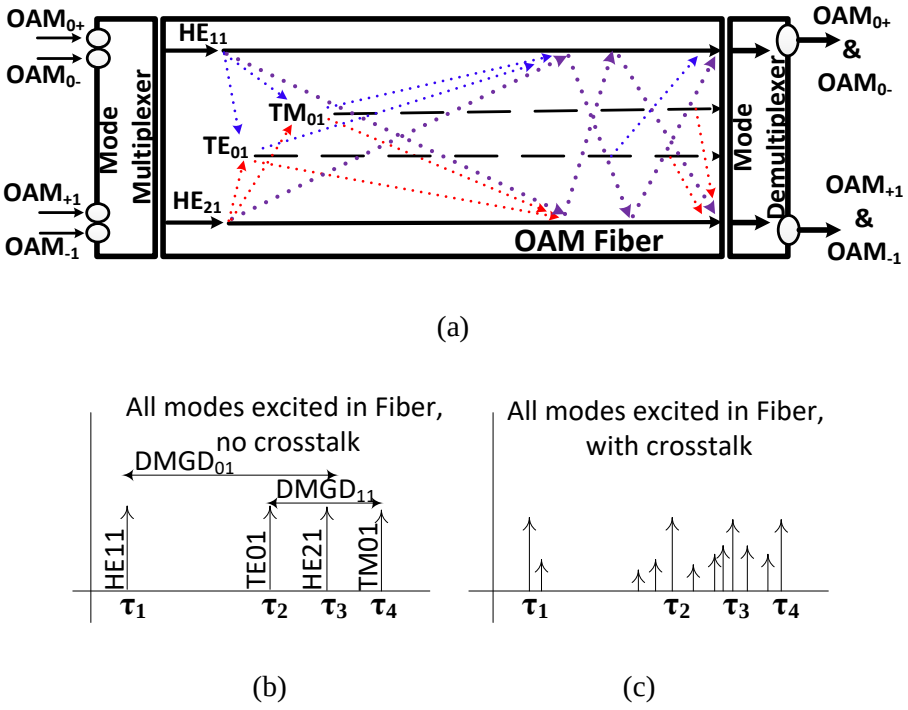

Fig. 4.1. (a) Channel model for interactions among vector modes propagating in OAM fibers supporting modes of order zero and one. Fiber output when launching a pulse in 4 supported vector modes (b) assuming no interaction among modes (c) with interactions among modes

between the excited HE_{11} and HE_{21} modes, as well as leakage from these excited modes to and from the parasitic TE_{01} and TM_{01} modes.

In OAM fibers, to reduce receiver complexity, the effective index separation between $HE_{|l|+1}$ and $EH_{|l|-1}$ modes is maximized to minimize coupling and crosstalk.

The effective indices of TE_{01} and TM_{01} modes are also separated from that of HE_{21} to avoid formation of LP modes. Each vector mode has a distinct propagation constant and there is low coupling among modes. Assuming no crosstalk and launching a short pulse simultaneously on all 4 modes in an OAM fiber supporting modes of order zero and one leads to four pulses with distinct arrival times (related to their group velocities) at the fiber output, see Fig. 4.1(b). Possible leakage paths are illustrated in dotted lines in Fig. 4.1(a). In Fig. 4.1(c), we observe the effect of crosstalk, where launching a pulse in all the four modes can generate any number of pulses at the fiber output.

In an OAM transmission system with separate mode detection, the mode demultiplexer is followed by two isolated and uncoordinated receivers: one for $OAM_0^{\pm}$ and one for $OAM_{\pm1}$. There is no receiver for the TE_{01}/TM_{01} modes. The two isolated receivers will detect signals propagating along the direct path, but they will also receive leakage from other modes and the leakage from the same mode that goes back and forth between modes causing both interference (from the alternate information channel) and intersymbol interference (from the primary information channel).

The effective indices of TE_{01}/TM_{01} modes are close to HE_{21} in OAM fibers. Therefore, the interactions between [TE_{01}/TM_{01} and HE_{21}] tend to be stronger than both the crosstalk between [HE_{11} and HE_{21}] and the interactions between [HE_{11} and TE_{01}/TM_{01}]. Throughout this chapter, we use $DMGD_{01}$ for the DMGD between HE_{11} and HE_{21} modes and $DMGD_{11}$ for the DMGD among vector modes HE_{21}, TE_{01} and TM_{01} that constitute OAM mode group one (OAM_1).

To study the impact of modal impairments, we examine RCF and IPGIF fibers, each supporting OAM modes of order zero and one. RCF is a step index fiber described in detail in [59], while IPGIF is a graded index fiber with an inverse parabolic index profile described in detail in [60]. Each fiber has distinct effective index separations among vector modes and distinct crosstalk levels and $DMGD_{01}$ and $DMGD_{11}$. The numerical aperture of the RCF and IPGIF fibers are 0.2959 and 0.1702, respectively. The loss of fibers using OTDR measurement without selective modal excitation at 1550 nm was measured as 3.8 dB/km and 2.8 dB/km for IPGIF and RCF, respectively. In next sections, we characterize

the OAM-MDM link to observe and quantify the modal impairments in our OAM-MDM system.

4.3. OAM-MDM Link Characterization

In this section, we present ToF and IR measurements for an OAM-MDM system. These two experiments can give the same results in LP-MDM systems but in OAM-MDM systems using modes of order one, they will not give the same results. ToF measurement characterizes the interactions among all the supported vector modes during fiber propagation. This includes all the vector modes of HE_{11}, HE_{21}, TE_{01} and TM_{01}. IR characterizes the coupling among modes used as data channels in the OAM-MDM link, i.e HE_{11} and HE_{21}. In ToF experiments, we intentionally excite all vector modes (HE_{11}, HE_{21}, TE_{01} and TM_{01}) to observe the interactions among them during fiber propagation. In IR, we selectively excite and receive HE_{11} and HE_{21} modes using a mode mux and demux and observe the interactions between them. In IR measurements, however, power leakage leads to interactions among HE_{21} and TE_{01}/TM_{01} modes during fiber propagation and the powers that goes to TE_{01}, TM_{01} modes and come back to HE_{21} will be captured by this method.

4.3.1. Time of flight measurements

In Fig. 4.2, we present the ToF setup used to measure the DMGD among vector modes. A pulse train with 40 ps pulse width and 51.2 ns repetition rate is generated by externally modulating a continuous-wave (CW) laser source in a Mach-Zehnder optical intensity modular. This signal is directed via free space optics to a forked grating on a glass plate that generates an OAM_{+1} mode. Off-axis coupling to the fiber excites *all* supported vector modes simultaneously. The fiber output is detected by a high speed photodetector and recorded using a digital sampling oscilloscope (DSO) and presented in Fig. 4.3(a) for IPGIF and Fig. 4.3(b) for RCF. We adjusted the off-axis alignment until pulses with comparable power levels for all supported vector modes were observed. In both fibers, we observe four peaks corresponding to HE_{11}, TE_{01}, HE_{21} and TM_{01} modes, as labeled in

Fig. 4.3(a) and 4.3(b). Vector modes arrive at different times as they have different group velocities. DMGD between vector modes are calculated from temporal separation of peaks in Fig. 4.3(a) and 3(b) and reported in Table 4.1. Comparing the two fibers, RCF has larger $DMGD_{11}$ and smaller $DMGD_{01}$ than IPGIF. A prominent pedestal response is observed among TE_{01}, HE_{21} and TM_{01} in both fibers due to modal interactions; these modes continuously exchange power during propagation. The width of this pedestal is a little larger than $DMGD_{11}$. The impact of this pedestal on OAM-MDM performance will be investigated in later sections.

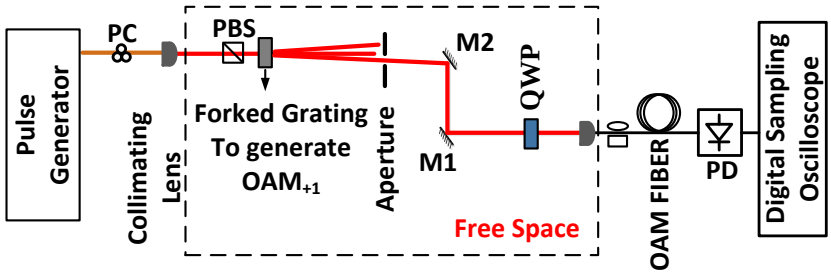

Fig. 4.2. Setup for Time of flight measurement

Table 4.1. Measured DMGD between OAM0 and OAM1 mode groups per fiber

Fiber	DMGD (ns) ±0.1 ns			
	($DMGD_{01}$) HE_{11} – HE_{21}	HE_{21} – TM_{01}	TE_{01} – HE_{21}	($DMGD_{11}$) (HE_{21} –TM_{01}) + (TE_{01} – HE_{21})
1.1 km IPGIF	31.2	0.5	1.2	1.7
1.47 km RCF	23.9	1.2	2.6	3.8

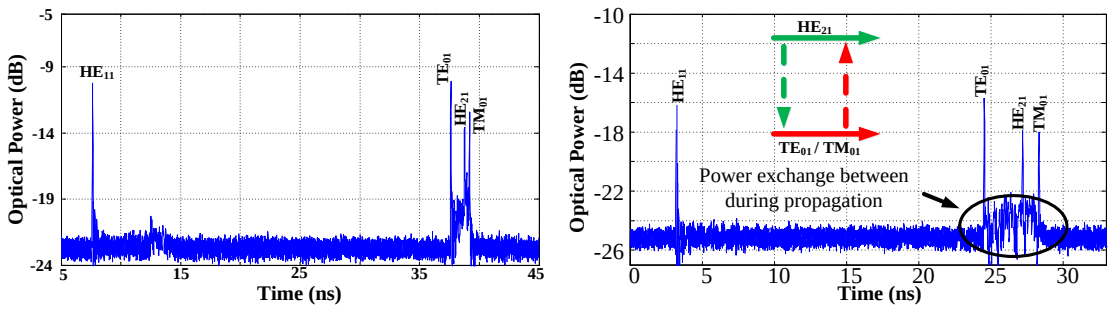

(a) (b)

Fig. 4.3. ToF measurement results, (a) IPGIF (b) RCF

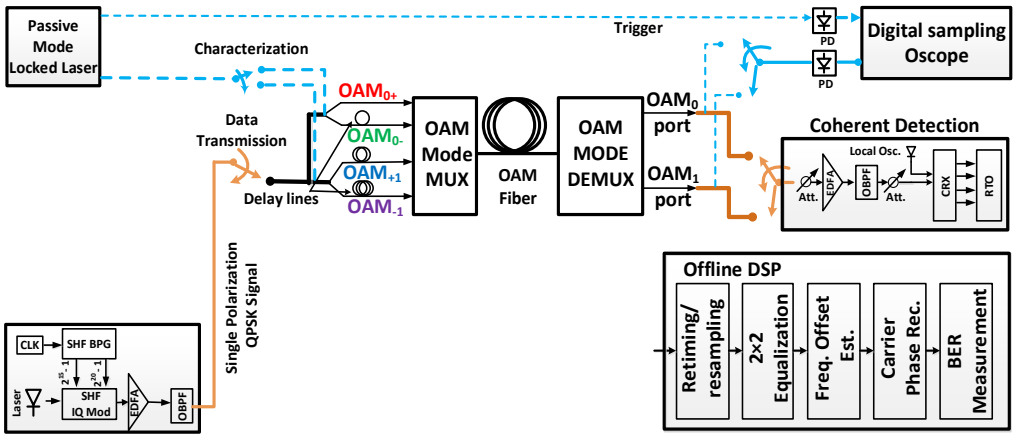

Fig. 4.4. OAM-MDM characterization and data transmission setup

4.3.2. Channel impulse response

We measured channel impulse responses with the experimental setup in Fig. 4.4 with input and output connections in blue dashed lines. A passive mode locked fiber laser generates pulses with duration of ~10 ps with repetition rate of 50 ns. The demux output ports are captured by a DSO. We launched pulses on one channel at a time and recorded each demux output port. The technique of capturing one mode at a time in channel characterization was already discussed in [62]. Sixteen impulse responses measured for each fiber are shown in Fig. 4.5 and 4.6, arranged in a 4×4 channel matrix configuration; launched modes form columns, and received modes form rows. Some submatrices are magnified to better show the details.

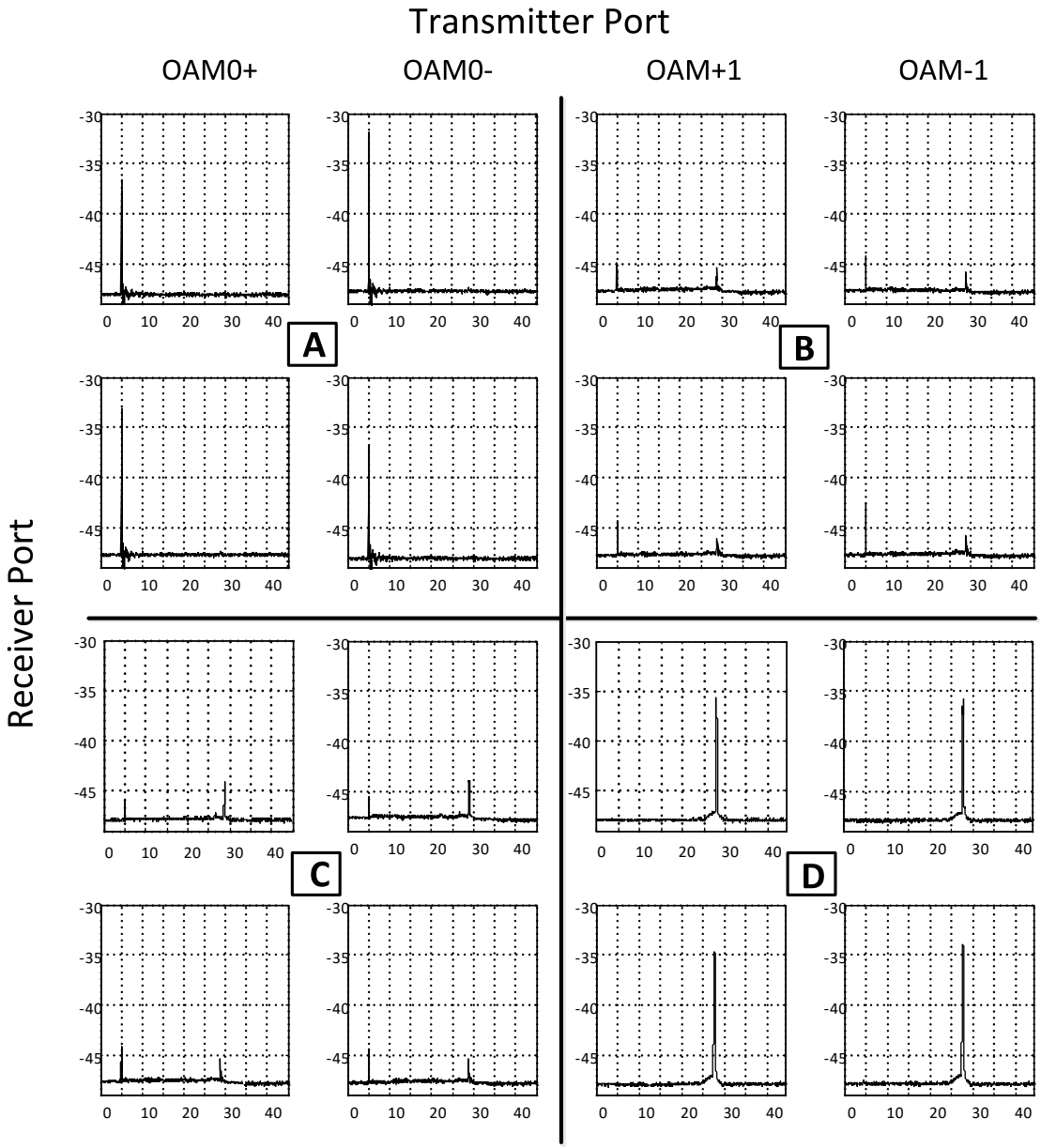

Fig. 4.5. Channel impulse response for OAM-MDM link using a 1.47 km RCF with scales of (dB) and (ns) on x and y axes of sub figures.

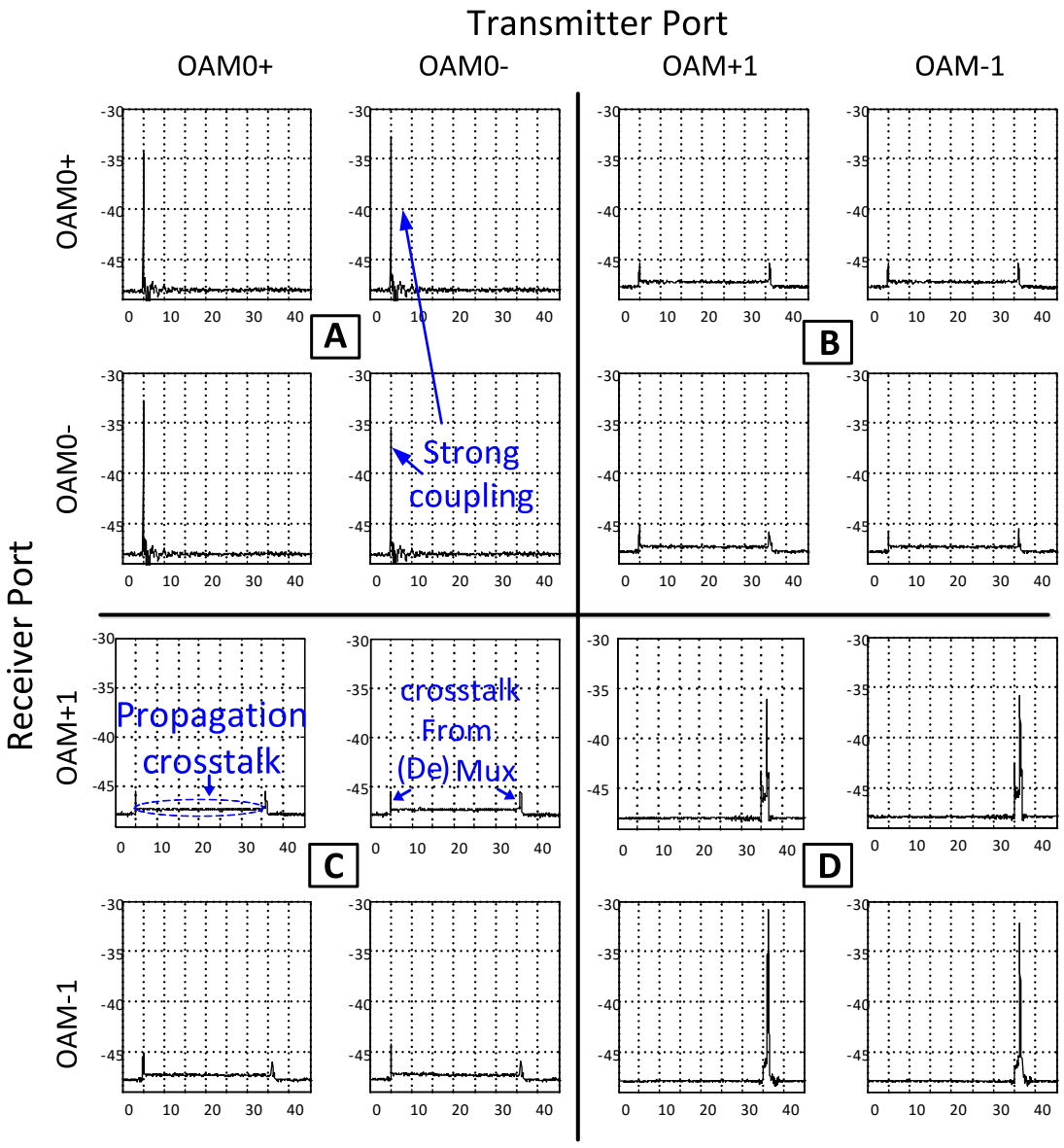

Fig. 4.6. Channel impulse response for OAM-MDM link using a 1.2 km IPGIF with scales of (dB) and (ns) on x and y axes of sub figures.

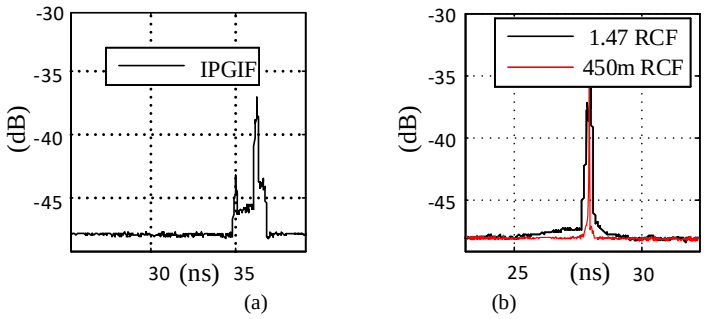

Fig. 4.7. Enlarged channel impulse response for case of sending and receiving OAM +1 in (a) 1.2 km IPGIF (b) 1.47km and 450 m RCF

The channel matrix is divided to four subsections for each fiber, labeled A through D. The 2×2 diagonal subsections (A and D) show interactions within each mode group, i.e., [OAM_0^+ with OAM_0^-] and [OAM_{+1} with OAM_{-1}]. The off-diagonal subsections (B and C) show interactions across mode groups. Since the channels inside each mode group are degenerate, there is strong coupling peaks in subsections A and D. For off-diagonal subsections, we observe two contributions to crosstalk: i) coupling at mux or demux appearing as sharp peaks, and ii) fiber coupling distributed over time that occurs throughout propagation.

In off-diagonal submatrices, B and C, the crosstalk from one mode group to the other is depicted. By comparing submatrices B and C for the two fibers, we observe more propagation crosstalk in IPGIF than RCF. We suspect the higher distributed mode coupling in IPGIF to be due to effects such as micro bending or fabrication imperfections.

We observe pulse broadening in subsection D for $OAM_{\pm1}$ modes, while the pulses remain sharp for OAM_0 in subsection A. Enlarged impulse responses of fibers for case of sending and receiving OAM_{+1} are depicted in Fig. 4.7. The width of measured pulses are 2.1 ns for IPGIF, 4.9 ns for 1.47 km RCF; width is calculated for values above the noise floor. These pulse widths are close to $DMGD_{11}$ measured by ToF, 1.7 ns for IPGIF and 3.8 ns for 1.47 km RCF. Using a full width 0.1 maximum definition, the IPGIF pulses are more broadened with a 2 ns width compared to 1.47 km RCF with a 0.6 ns width.

4.3.3. Crosstalk Measurements

To complement IR measurements, we also measure total crosstalk among mode groups. Crosstalk measurement is done with the same signal source used for data transmission: a 16 Gbaud QPSK signal on two polarizations (setup described in detail in the next section).

We used a power meter to measure the received power at demultiplexer output port when transmitting two polarizations of the corresponding or the other mode group. The crosstalk can be calculated similar to the method explained in section 3.4 with equation (1.3). Results are reported in Table 4.2. Crosstalk is lower in RCF, consistent with IR matrices. We also measured the crosstalk from MUX and DEMUX stages using a 1m RCF fiber, where the propagation crosstalk in the fiber is negligible. This crosstalk was around -20 dB.

Table 4.2. Measured crosstalk (dB) among OAM modes in OAM-MDM link for 1.47 km RCF and 1.1 km IPGIF

IPGIF	$HE_{11} \Rightarrow HE_{21}$	-7.7	$HE_{21} \Rightarrow HE_{11}$	-7.3
RCF	$HE_{11} \Rightarrow HE_{21}$	-10.7	$HE_{21} \Rightarrow HE_{11}$	-10.6

4.3.4. Interpretation of system characterizations

In ToF, we excited all vector modes and observed a pedestal response among HE_{21} and TE_{01}/TM_{01} due to continuous interactions among these vector modes during propagation. In IR measurements, we launched one targeted mode at a time, i.e., $OAM_0^{\pm}$ or $OAM_{\pm1}$, and captured each demux output. In IR measurements, the pulse in $OAM_{\pm1}$ modes is broadened with a width similar to the ToF pedestal width. We conclude pulse broadening is due to power exchange within mode group one: HE_{21} leaking to/from parasitic modes TE_{01} and TM_{01}. This modal mixing can occur in fiber or mode (de)mux. Note that, unlike the ToF setup, in IR measurement, we do not excite TE_{01} and TM_{01} modes. Their effect is inferred from the pulse broadening in HE_{21} mode matching the pedestal width in ToF measurements. The parasitic modes of TE_{01}/ TM_{01} may be incidentally excited during mux

and/or demux; they may arise during coupling in the fiber propagation. The reason that the pedestal around HE_{21} has a higher power level in ToF compared to IR is that, in ToF, TE_{01} and TM_{01} are intentionally excited at the input of fiber with the power comparable to HE_{21}. This observation means that although TE_{01}/TM_{01} modes are not used as data carrying channels, they can affect receiver performance by pulse broadening in $OAM_{\pm1}$ modes resulting in intersymbol interference (ISI) among consecutive data symbols transmitted in $OAM_{\pm1}$ channels. Such phenomena can affect the memory depth requirement for receiver equalizers. It will be discussed in the next section via data transmission results.

4.4. Data Transmission in OAM-MDM link

In this section, we discuss data transmission results for four channels ($OAM_0^{\pm}$ and $OAM_{\pm1}$) over RCF and IPGIF fibers. In section A, we briefly describe the data transmission setup. In Section B, we evaluate the receiver BER and discuss the impact of modal impairments on system performance and equalizer memory depth for RCF and IPGIF fiber. In section C, we examine RCF fiber of different lengths.

4.4.1 Data transmission setup

Fig. 4.3 shows the data transmission setup; input switches are set for data and output switches are set for coherent detection. A single polarization non-return-to-zero (NRZ) QPSK signal at baud rate of 16 Gbaud is generated via a bit pattern generator (BPG) with two pseudo random binary sequences (PRBS) of length 2^{15}-1 and 2^{20}-1 and an MZM IQ modulator. The transmitter laser has a linewidth of 100 kHz and is set to 1550 nm with output power of 16 dBm; the generated QPSK signal is amplified and then sent to the OAM-MDM link.

By using delay lines, four decorrelated replicas of the signal are generated. These four decorrelated signals are input to a mode multiplexer where two of them are mapped on $OAM_{\pm1}$ modes and combined with the two on $OAM_0^{\pm}$ mode. They are then coupled to the OAM fiber. After propagation over OAM fiber, the two mode groups are separated in the

polarization diverse mode demultiplexer and sent to data recovery setup separately. A single coherent receiver (CRX) with bandwidth of 22 GHz and a local oscillator with linewidth of 10 kHz and output power of 13 dBm are used to coherently detect the incoming signal, either two polarizations of OAM_0 or $OAM_{\pm1}$. The output electrical signals from the coherent receiver are captured by a Keysight real-time oscilloscope (RTO) with 33 GHz analog bandwidth capturing data at 80 Gsample/s; afterwards the DSP is applied offline. The offline DSP is the same as that used in dual-polarization, single-mode coherent detection, including blocks of resampling, 2×2 equalization between two polarizations of each mode, frequency offset estimation and carrier phase recovery.

4.4.2. BER and required memory depth for RCF and IPGIF

We ran data transmission, evaluated BER and determined required memory depth in two scenarios - sending only one mode group (two channels) or sending all channels. BER estimation at each point in the curve was done over 10^6 samples captured during a single transmission. Transmitting only one mode excludes the impact of crosstalk across mode groups. Sections A and D of channel matrices apply to sending only $OAM_0^{\pm}$ and $OAM_{\pm1}$ respectively. BER versus number of taps per equalizer are presented in Fig. 4.8 (a) and (b) for $OAM_0^{\pm}$ and $OAM_{\pm1}$, respectively. When sending only $OAM_0^{\pm}$, we do not observe any meaningful BER dependency on equalizer memory depth; even small equalizer lengths reach the minimum of BER for both fibers. The minimum achievable BER is the same for both fibers. When sending only $OAM_{\pm1}$, we reach the minimum of BER with 20 and 90 half-symbol-spaced taps for RCF and IPGIF, respectively, corresponding to 0.625 ns and 2.8 ns. The required equalizer memory depth is due to pulse broadening in $OAM_{\pm1}$ channels. Increasing the number of equalizer taps compensates for ISI due to pulse broadening.

Next, we report in Fig. 4.9, the BER versus number of taps when sending both mode groups (all 4 data channels). Fig. 4.9 (a), (b) show the BER at the receiver for the zero and one order modes, respectively. Comparing Fig. 4.8 (one mode at a time) and Fig. 4.9 (all modes), achievable BER is lower and there is an OSNR penalty to reach that BER. Note that the measurements in Fig. 4.8 and Fig. 4.9 are evaluated at OSNRs of 16 dB and 25 dB,

respectively. When sending all channels, regardless of memory depth used, RCF fiber always outperforms IPGIF on all data channels due to lower crosstalk.

For $OAM_0^{\pm}$, Fig. 4.9(a), we again observe no BER dependency on equalizer memory depth. For $OAM_{\pm1}$, Fig. 4.9(b), beside the OSNR penalty, we observe more required taps for both fibers to reach the minimum of BER compared to the crosstalk-free case of Fig. 4.9(b). We reach the minimum of BER with 160 taps (5 ns) for IPGIF and 170 taps (5.3 ns) for RCF. The reason for increased number of taps, compared to the case of sending only $OAM_{\pm1}$, is the crosstalk from $OAM_0^{\pm}$ channels as discussed in the next section.

4.4.3. BER and required memory depth for two lengths of RCF

To further investigate the impact of crosstalk from $OAM_0^{\pm}$ on equalizer memory depth in $OAM_{\pm1}$ channels, we examine a 0.45 km RCF fiber with crosstalk of -15.5 dB between $OAM_0^{\pm}$ and $OAM_{\pm1}$. $DMGD_{01}$ and $DMGD_{11}$ can be inferred from the 1.47 km fiber measurement using the ratio of fiber lengths ($0.45/1.47 \approx 0.3$). $DMGD_{11}$ is about1.26 ns for the shorter fiber. In Fig. 4.10, we compare BER performance for $OAM_{\pm1}$ channels for these two RCF lengths. The required memory depth to reach minimum BER for 0.45 km fiber is around 15 taps or ~0.47 ns, which is smaller than its $DMGD_{11}$. The required memory depth for 1.47 km fiber at minimum BER is around 160 or 5 ns, which is larger than its $DMGD_{11}$. In next section, we discuss the relationship between memory depth requirement and modal interactions observed in section 4.3.

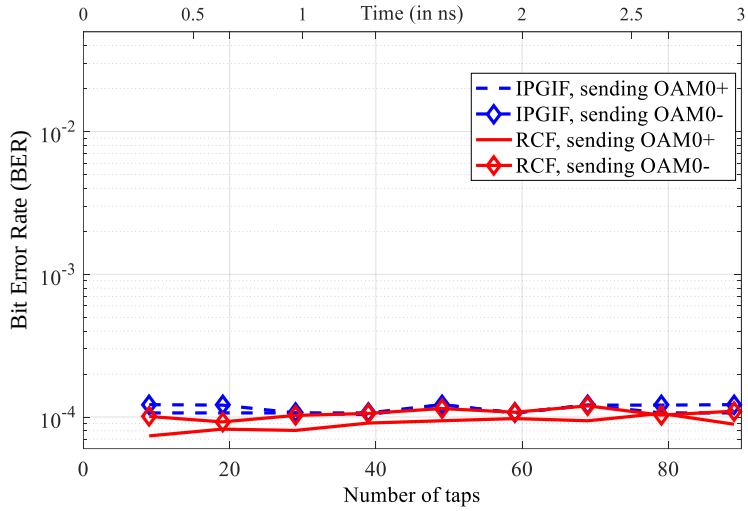

(a)

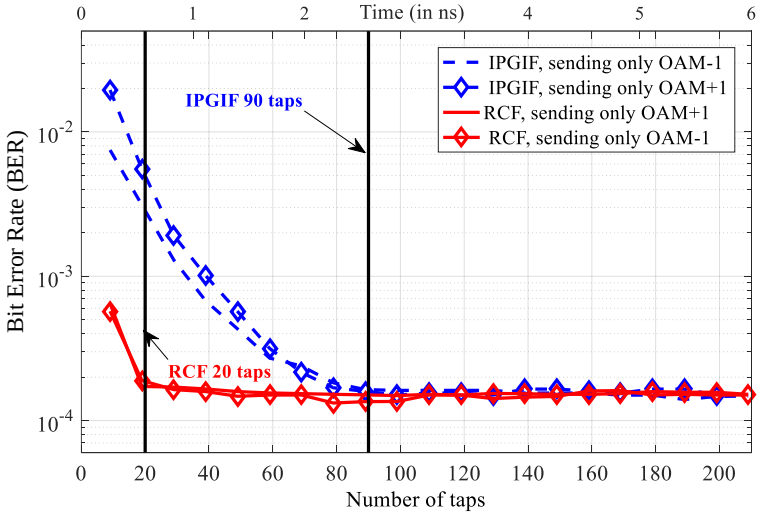

(b)

Fig. 4.8. BER at OSNR = 16 dB vs. number of taps, (a) sending only OAM0, (b) sending only OAM±1; Length of IPGIF and RCF are 1.2km and 1.47 km, respectively.

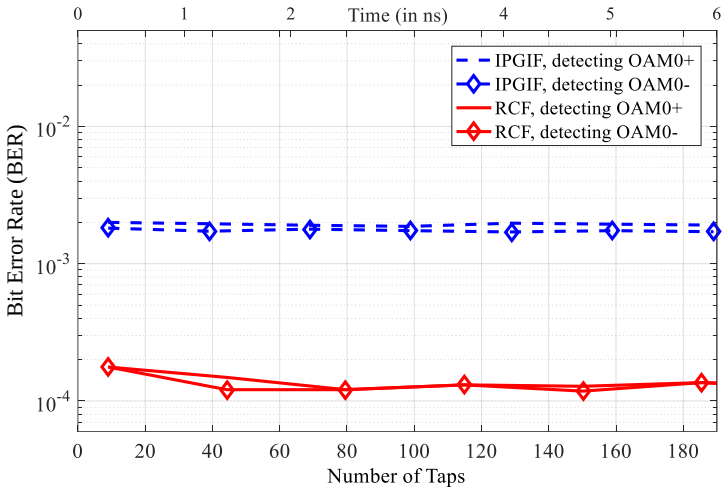

(a)

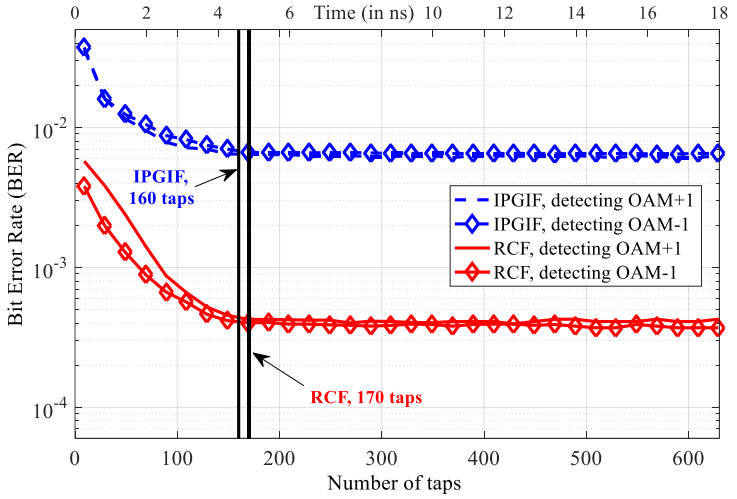

(b)

Fig. 4.9. BER at OSNR = 25 dB vs. number of taps, sending all modes and (a) detecting OAM0, (b) detecting OAM±1; Length of IPGIF and RCF are 1.2km and 1.47 km, respectively.

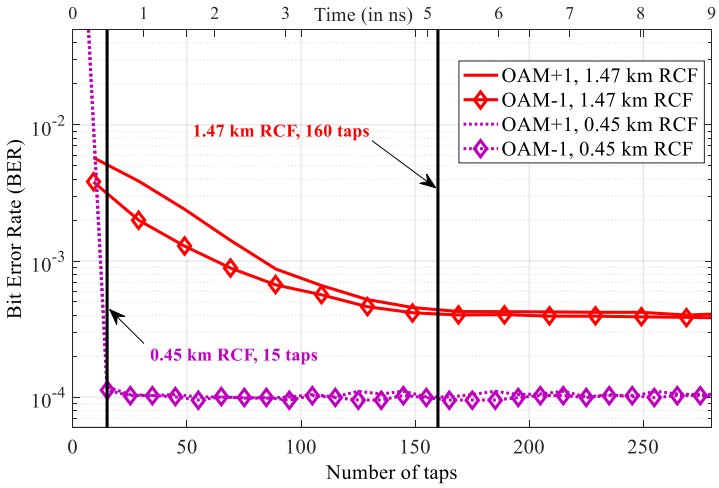

Fig. 4.10. BER vs number of taps for OAM±1 channels, RCF fibers of 1.47 km at OSNR=25 dB and 450 m at OSNR=16 dB

4.5. Discussion on receiver performance and complexity

We summarize the parameters related to receiver complexity for $OAM_{\pm 1}$ channels that were estimated in experiments in Table 4.4. In the first column, we have the crosstalk from $OAM_0^{\pm}$ on $OAM_{\pm 1}$. In the other columns are time constants measured first in characterizing the fibers and then via BER evaluation (equalizer memory depth).

Consider RCF and IPGIF at lengths above a kilometer. The pulse broadening (Fig. 4.7) when measured as all points above the noise floor is reasonably close to $DMGD_{11}$ measured in ToF (Fig. 4.3). $DMGD_{11}$ measures time between peaks, but not the edges of the interactions on either side of these peaks, hence it is natural that $DMGD_{11}$ is smaller than the pulse broadening. This time constant is closely related to the equalizer memory depth when sending all modes (darker shading on these values).

Pulse broadening at full width 0.1 maximum is a close match to memory depth of equalizers when sending only $OAM_{\pm 1}$, i.e., with no crosstalk present (lighter shading on these values). We probed the level of broadening having significant impact on DSP complexity, and settled on the 0.1 maximum value.

The interactions among TE_{01}/TM_{01} and HE_{21} are the primary source of intersymbol interference, as data moves between the three vector modes. These strong modal interactions lead the full width 0.1 maximum pulse broadening of IPGIF to be nearly equal to the noise floor broadening measurement; the broadened pulse is nearly rectangular. With lower interactions in RCF, the broadened pulse rolls off more slowly.

When sending only $OAM_{\pm1,}$ crosstalk is absent and ISI is the only impairment to overcome. Hence, the equalizer memory depth is determined by a time constant nuanced with the level of interaction within the mode group, i.e., the full width 0.1 maximum pulse broadening. Note that equalizer memory depth will always be larger than the relevant time constants to compensate the other impairments as well (e.g., imperfect sampling, limited RF bandwidth, limited sample resolution, etc.) [63], [64].

Table 4.3. Summary of parameters in characterization and data transmission related to memory depth of equalizers

	Characterization measurements				Data transmission	
Fiber	crosstalk	ToF	impulse response		equalizer memory depth	
	HE_{11} on HE_{21}	$DMGD_{11}$	pulse broadening: noise floor	pulse broadening: 10dB	sending only $OAM_{\pm1}$	sending all modes
RCF 1.47 km	-10.5 dB	3.8 ns	4.9 ns	0.6 ns	0.62 ns	5.3 ns
IPGIF 1.10 km	-7 dB	1.7 ns	2.1 ns	2.0 ns	2.8 ns	5 ns
RCF 0.45 km	-15.5 dB	1.26 ns	0.4 ns	0.3 ns	–	0.5 ns

When sending all channels and detecting $OAM_{\pm1}$, crosstalk from $OAM_0^{\pm}$ is present as well as ISI. The memory depth is increased as the equalizer uses more taps to gather energy from the desired signal to overcome crosstalk. The relevant time constant is now the $DMGD_{11}$. The equalizer scavenges all available traces of the desired signal in the isolated, single port to which it has access. By exceeding the $DMGD_{11}$ (which measures time between peaks, but not the edges of the interactions on either side of these peaks), our

equalizers collect signal energy in HE_{21} that goes to TE_{01}/TM_{01} and HE_{11} and comes back to HE_{21} in the enlarged time span. Furthermore, by using a higher memory depth, the errors due to pulse broadening from a larger number of adjacent symbols will be corrected. Without full MIMO, i.e., without access to data leaked to the unobserved port, the receiver has very limited improvement for memory depth significantly beyond $DMGD_{11}$, as seen in the BER floor.

Finally, we compare the two RCF fibers of length 0.45 km and 1.47 km. The $DMGD_{11}$ scales linearly with fiber length, but equalizer memory depth is more than 10 times larger for the longer fiber. The crosstalk is more than 3 times larger in the longer fiber. This reinforces our argument that larger crosstalk leads to memory depth greater than $DMGD_{11}$. In the shorter fiber where the BER penalty due to crosstalk is negligible, the memory depth is much smaller (.5 ns) than $DMGD_{11}$, (1.26 ns). Tap number reduction exceeding the ratio of RCF lengths can be attributed to differences in pulse broadening. In Fig. 4.7(b), where pulse broadening in 1.47 km and 450m RCF is depicted, tails of the impulse response at 450 m are much less extensive than those in the longer fiber; at 450 m the pulse broadening gives very consistent figures of merit (10dB pulse width or noise floor pulse width).

Time domain equalization was used to facilitate interpretation of results, in particular the relevance of time constants observed in our ToF and impulse response characterizations. A practical system would use frequency domain equalization for memory depth greater than 16 taps [65].

4.6. Conclusion

We observed different memory depth requirements in reception of data carried by OAM modes of order zero and one. We investigated the source of this difference via channel characterization and data transmission. Unlike LP-MDM, TE_{01}/ TM_{01} modes are not data carrying for OAM-MDM. These modes are nonetheless incidentally excited, and therefore become parasitic modes in the fiber, interacting with data carrying modes. Their interaction with HE_{21} can result in pulse broadening and ISI for data transmitted in $OAM_{\pm1}$ channels. Results shows that memory depth of equalizers in $OAM_{\pm1}$ channels is directly related to

this phenomenon, as well as channel crosstalk. For OAM-MDM systems targeting a low complexity receiver, the interactions between data carrying HE_{11} and HE_{21} modes and non-data carrying TE_{01}/ TM_{01} should be minimized in fiber design. If this is not possible, higher order modes may be more appropriate as their interaction with parasitic modes would be much reduced.

Chapter 5

Data Transmission over Linearly Polarized Vector Modes of a Polarization Maintaining Elliptical Ring Core Fiber

Résumé - Pour la première fois, nous rapportons la transmission de données sans MIMO sur 6 modes vectoriels dans une fibre à noyau elliptique à maintien de polarisation (ERCF) dans un schéma de détection cohérent. C'est la base pour une étude expérimentale de la faisabilité de la transmission de signaux radiofréquence (RF) sur un ERCF de maintien de polarisation de 900 m. Aucun traitement de sortie multiple à entrées multiples (MIMO) n'est utilisé pour récupérer les signaux RF portés par différents modes; nous récupérons le 16QAM, multiplexage par répartition orthogonale de la fréquence (OFDM) signaux RF avec les mêmes techniques utilisées pour les fibres monomodes. Pour la première fois, nous rapportons la transmission de quatre flux RF sur quatre canaux dans une fibre à quelques modes. En outre, pour la première fois, nous transmettons des signaux RF sur deux polarisations d'un mode dans les fibres à modes et restituons avec succès les données dans les deux polarisations sans suivi de polarisation ou traitement de signal numérique pour séparer les polarisations. En outre, nous examinons l'impact de la flexion de la fibre sur la diaphonie entre les canaux. Nous montrons que même en cas de forte flexion, les états de polarisation restent séparés et les flux RF transmis sur les états de polarisation d'un mode pourraient être récupérés avec une pénalité de faible puissance. Les résultats d'expériences cohérentes et non cohérentes sont comparés et contrastés.

Abstract - For the first time, we report MIMO-free data transmission over 6 vector modes in polarization-maintaining elliptical ring core fiber (ERCF) in a coherent detection scheme. This is the baseline for the experimental investigation of the feasibility of transmission of radio frequency (RF) signals over a 900 m polarization-maintaining ERCF. No multiple-input multiple output (MIMO) processing is used to recover the RF signals carried by

different modes; we recover the 16QAM, orthogonal frequency division multiplexing (OFDM) RF signals with the same techniques used for single mode fibers. For the first time, we report transmission of four RF streams over four channels in a few mode fiber. Also, for the first time, we transmit RF signals over two polarizations of a mode in few mode fibers and successfully recover data in both polarizations without polarization tracking or digital signal processing to separate polarizations. Furthermore, we examine the impact of fiber bending on crosstalk between channel. We show that even under severe bending, the polarization states remain separated and the RF streams transmitted on polarization states of a mode could be recovered with low power penalty. The results of coherent and non-coherent experiments are compared and contrasted.

5.1. Introduction

Extensive research is underway for novel radio over fiber (RoF) technologies [66]. The number of wireless network users is increasing annually; popular mobile applications exploit high bandwidth connections, leading to intensified demand [67]. The use of 64 antennas per sector is planned, so called massive multiple input, multiple output (MIMO), but will put a great burden on optical front-haul. 5G is heading for a tremendous capacity shortfall in RoF front-haul.

Different multiplexing techniques in optical systems used in RoF architectures have been proposed to cope with future traffic demands on wireless networks. Polarization division multiplexing (PDM) offers a two-fold increase in capacity of single mode systems, but requires optical polarization tracking or relies on additional MIMO processing for joint optical/wireless channel [68], [69]. Wavelength division multiplexing (WDM) [70-72] can increase the capacity, but cost is high if wavelengths must be densely packed.

In space division multiplexing (SDM), based on multimode fibers (MMF), few mode fibers (FMF) or multicore fibers (MCF), capacity is scaled by the number of modes/cores exploited. As a rule of thumb, MMF sees the greatest interaction (i.e., model mixing causing crosstalk) among channels, while MCF sees the lowest. FMF interactions depend widely on the fiber used. MIMO algorithms in digital signal processing (DSP) at reception can mitigate interactions, at the cost of greater DSP complexity. We review the use of RoF with all fiber types.

The feasibility of RoF over MMF was investigated via characterization techniques in [73]. Two and three modes in conventional MMF were used for RoF data transmission in [74] and [75], respectively, but required MIMO processing. At the other end of the spectrum, MCFs have low inter-core crosstalk, whose impact on RoF was studied in [76], [77]. RoF systems using 2, 4 or 6 cores of MCF with low modal mixing were demonstrated [78-81].

As SDM capacity can be pushed by having multiple cores supporting a few modes per core, the study of FMF for this application is of interest. Only limited RoF demonstrations on FMF have been reported. In [82] two RoF signals were transmitted over an elliptical core few mode fiber [83].

MIMO processing is being exploited in digital optical systems in FMF to separate modes and in wireless transmissions to separate antennas paths. The optical and wireless channels have vastly different characteristics. It remains to be established if the optical/wireless channel will suffer the capacity reduction identified for concatenated wireless channels in [84]. Rank deficiency was identified for these product channels, attributable to spatial correlation and lack of scattering richness. Instead of relying on MIMO for FMF transmissions, we focus on FMF with low modal mixing [85-89]. These FMF did not require MIMO processing for digital transmissions. Spatial multiplexing that does not require MIMO processing allows fiber capacity to grow in the spatial dimension without impinging on the capacity of the wireless channel, and is most appropriate for front-haul challenges.

In this chapter, we will investigate the feasibility of RoF transmission over a polarization-maintaining elliptical ring core fiber (PM-ERCF) [90]. To facilitate comparison, we first run baseline experiments with wideband QAM and coherent detection, much as presented in the previous chapters. This will allow some discussion of relative performance of RoF and wideband QAM, as well as establishing the viability of MIMO-free data transmission in a coherent detection scheme over six linearly polarized vector (LPV) modes of ERCF. Both crosstalk among channels and BER after transmission are evaluated. The BER is found both for cases of sending only one channel or sending all the channels simultaneously.

Next we transmit, for the first time, RoF signals over four LPV modes of PM-ERCF. We demonstrate transmission of 4×1.152 Gbps 16QAM orthogonal frequency division multiplexing (OFDM) signals with direct detection and without MIMO processing over a 900 m fiber link. For the first time, we also exploit two polarizations of a mode for transmission of RoF signals over FMF. The data transmission experiment validates RoF signals mode division multiplexed (MDM) in FMF are recovered without intermingling of RoF data streams.

We characterize the RoF system in terms of crosstalk over spatial channels for signals with RF carriers ranging from 800 MHz to 6 GHz. We evaluate the bit error rate (BER) performance of the four RoF channels when centered at RF carriers of 2.4 GHz (WiFi) and at 3.3 GHz (a candidate carrier [91] for 5G). We also study the performance penalty due to varying levels of fiber modal crosstalk. By investigating the loss and crosstalk changes as a function of bending, we can comment on the polarization maintaining property of PM-ERCF.

The remaining sections of this chapter are organized as follows. In section 5.2, we discuss the fiber under test and our strategy for probing the isolation it affords between channels. In section 5.3, we describe the coherent detection setup and present results for crosstalk measurements and BER evaluation. In section 5.4, we discuss non-coherent RoF system including the setup, crosstalk characterization and data transmission. In section 5.5, we compare the results of the two sets of coherent and non-coherent data transmission. In section 5.6, we investigate the bending property of the fiber and in section 5.7, we conclude the chapter.

5.2. Multiplexing on vector modes

We exploit a few mode fiber (PM-ERCF) whose characteristics are detailed in [89]. This fiber is designed to support the propagation of vector modes (fiber Eigen-modes) that are linearly polarized, and whose effective indices are sufficiently separated to suppress modal interactions. All FMF to date have polarizations that mix within the modes. PM-ERCF is designed and achieves the polarization maintaining property for higher order Eigen-modes, while the fundamental mode polarizations mix as in standard FMF. The PM-ERCF

supports eight channels: two polarizations in each of LPV_{01}, LPV_{11a}, LPV_{11b} and LPV_{21a} modes. We eschew the fundamental mode as it clearly would require MIMO processing for optical interactions, potentially leading to less capacity or greater complexity in the combined optical/wireless MIMO link. We focus on the higher order modes where polarization in maintained.

For the coherent detection experiment, all the supported vector modes with polarization maintaining property are used as data channels, i.e. $LPV_{11ax,y}$, $LPV_{11bx,y}$ and $LPV_{21ax,y}$. In RoF experiment, as we will report BER performances in section 5.4, we couldn't use all these six channels for data transmission because it will result in BER values higher than FEC threshold with 7% overhead. Therefore, we had to choose a strategy to exploit the maximum number of channels that could be transmitted with BERs below the FEC threshold while exploring the modal interactions of interest.

Table 5.1. Measured effective index separation between data carrying vector modes

$LPV_{11,a,x} \leftrightarrow LPV_{11,b,x}$	$LPV_{11,b,x} \leftrightarrow LPV_{11,b,y}$	$LPV_{11,b,y} \leftrightarrow LPV_{21,a,x}$
4.33×10^{-3}	3.07×10^{-4}	2.9×10^{-3}

One potential source of modal interaction is when RoF signals are carried by two polarizations of the same mode. The other is when we use different modes, either on the same or opposite polarizations. We wish to examine the isolation of RoF signals in each of cases, so we make a strategic choice of vector modes to be tested. To investigate the polarization multiplexing property, two polarizations of LPV_{11b} mode are employed. To probe modal isolation, we add one polarization on the higher order LPV_{21a} mode, and another polarization on a mode of the same order, but spatially orthogonal, i.e., the LPV_{11a} mode. In total therefore, we use $LPV_{11a,x}$, $LPV_{11b,x,y}$ and $LPV_{21a,y}$ modes as our four data carrying channels in RoF experiment. The measured effective index separation between these four channels are reported in Table I. These modes were selected as they had the best separation among the available supported modes.

5.3. Coherent Detection of wideband QAM

In this section, we report the setup for data transmission results of [90]. The results will be contrasted with RoF experiments in section 5.5. The signal generation and reception are very similar to the experiments done with RCF fiber in chapters 3 and 4. First, we briefly review all the three parts of signal generation, mode multiplexer/demultiplexer and signal reception for this experiment.

The setup for MIMO-free data transmission over 6 vector modes with QPSK modulation in a coherent detection scheme over 0.9 km ERCF is shown in Fig. 5.1. A single polarization non-return-to-zero (NRZ) QPSK signal is generated by an IQ modulator driven by two pseudo-random binary sequence (PRBS) signals with lengths of 2^{15}-1 and 2^{20}-1. The tunable laser (TL) has a linewidth of 100 kHz and is set to 1550 nm. The QPSK modulated signal is split into 6 channels which are then time delayed (τ_1 to τ_6 in Fig. 5.1) to emulate 6 independent QPSK signals.

Signals corresponding to $LPV11_{ax,y}$ are combined through a fiber-based polarization beam combiner (PBC) and then are sent in free space through a collimator and shaped by a phase plate before being coupled into the ERCF. The fiber-based polarization controller (PC) before collimator and the half wave plate (HWP2) are adjusted so that the two polarizations align with the major or minor axis of the ERCF. A similar signal path as that of the $LPV11_{ax,y}$ is used for the two $LPV11_{bx,y}$ channels but the corresponding phase plate is rotated by 90°. For $LPV21_{ax,y}$ modes, we used a spatial light modulator (SLM1) with two separate phase mask programmed on it to generate two polarizations of $LPV21_a$. After the SLM, the $LPV21_{ax,y}$ channels are combined in free space by using HWP1 and a polarization beam splitter (PBS) and coupled into the fiber. The beam splitter/combiner and quarter

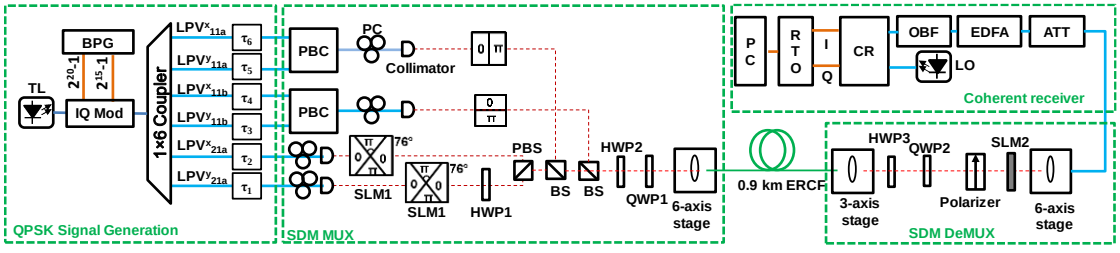

Fig. 5.1. Experimental setup for MIMO–Free 6 channels QPSK data transmission over PM-ERCF

wave plates are used to reject any spurious signal features resulting from non-ideal components. After propagating through a 0.9 km ERCF, the signals enter the demultiplexer stage. The demultiplexer consists of a half wave plate (HWP), a polarizer and a SLM. Proper HWP orientation and SLM programming allows us to select which channel will be demultiplexed. By rotating the HWP to ±45 degree, either *x* or *y* polarization is selected. By programming the SLM with the appropriate phase mask for the desired mode, that mode is converted to fundamental mode, while all other channels are shunted to higher order modes. The final demultiplexer stage is the SMF that acts as a mode stripper, allowing only the newly created fundamental mode to be detected. Undesired channels are rejected by the combined effects of the HWP, SLM and SMF. We test separate detection of each of the channels in a round-robin fashion.

For BER measurement, similar to the setup for RCF in section 3.3.1, we use noise loading with EDFA and attenuator so that the optical signal-to-noise ratio (OSNR) can be adjusted. The received signal is then directed to a coherent receiver with a bandwidth of 22GHz. As the optical local oscillator, a laser with linewidth of 10 kHz and output power of 13 dBm is used. Finally, the signal is captured by an RTO. To recover the signal, we use the offline DSP for single-polarization single-mode coherent detection systems already discussed in 2.2.1: blocks of resampling, an equalizer using CMA with 11 taps, frequency offset estimation and carrier phase recovery using 4^{th} power algorithm and BER calculation. No MIMO or PDM processing is used.

5.3.1. Crosstalk measurement for coherent detection scheme

Similar to the crosstalk measurements for RCF, we use a power meter to measure the received power at the demultiplexer output port. To calculate the crosstalk on channel *i*, *i* = 1,..,4, we set the HWP and SLM in the demultiplexer to receive channel *i* at the output port, i.e., creating output port *i*. We send, in turn, a 16 Gbaud QPSK signal on each of the six channels, measuring the power received. Let $P_{i,j}$ be the power at receiver port *i* when transmitting on mode *j*. The crosstalk for channel *i* is calculated as

$$\text{Crosstalk on channel } i = \frac{\sum_{j=1, i\neq j}^{4} P_{i,j}}{P_{i,i}} \tag{5.1}$$

Table 5.2 shows the measured power transfer matrix of 6 channel MDM system carrying QPSK signals. Note that crosstalk in Table 5.1 include crosstalk at fiber propagation and the mode multiplexer and demultiplexer.

Table 5.2. Received modal power matrix for coherent data transmission over 6 vector modes in (dB); columns are transmitted modes and rows are received modes

	$LPV_{11a,x}$	$LPV_{11a,y}$	$LPV_{11b,x}$	$LPV_{11b,y}$	$LPV_{21a,x}$	$LPV_{21a,y}$	Total Crosstalk (dB)
$LPV_{11a,x}$	-1.46	-14.25	-17.43	-27.32	-15.65	-22.35	-8.97
$LPV_{11a,y}$	-15.92	0	-25.55	-16.91	-19.45	-15.55	-10.56
$LPV_{11b,x}$	-16.75	-25.13	-1.88	-23.23	-14.37	-25.95	-9.79
$LPV_{11b,y}$	-26.95	-15.58	-25.16	-0.87	-26.55	-13.65	-10.20
$LPV_{21a,x}$	-15.45	-21.45	-15.95	-26.86	-1.42	-17.73	-9.55
$LPV_{21a,y}$	-21.76	-14.11	-26.74	-15.15	-17.1	-0.87	-9.23

5.3.2. BER evaluation in coherent detection

We transmitted QPSK signals at baud rate of 24 Gbaud in all the six vector modes and measured BER to evaluate the performance of the MDM system shown in Fig. 5.1. BER versus optical signal-to-noise ratio (OSNR) is depicted in Fig. 5.2 for the transmission of one mode at a time (colored solid lines) and the simultaneous transmission of all six modes (dashed lines with markers). BER estimation at each point in the curve was done over 10^6 samples captured during a single transmission. We could reach BER values below FEC threshold for all the six channels. An OSNR penalty around 8 dB at the FEC threshold of 3.8×10^{-3} was observed.

The BER performance of six channels transmitted over PM-ERCF in Fig. 5.2 prove the viability of MIMO-free data transmission over this fiber. For LPV modes, supported by PM-ERCF, the crosstalk between different modes is small; it’s also polarizations

maintaining resulting in low crosstalk from polarizations of a mode on each other. This fact results in further simplification of the receiver and equalizer structure compared to the structure used for OAM fibers. DSP of single mode single polarization systems, discussed in section 2.2.1 is used to recover the data in each of LPV modes.

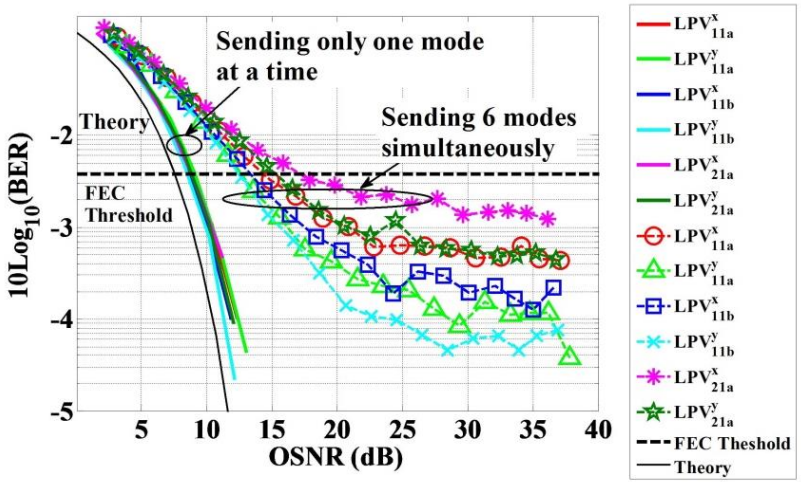

Fig. 5.2. BER versus OSNR for six channels data transmission over PM-ERCF at 24 Gbaud

5.4. Direct detection of Narrowband RoF OFDM

In this section, we describe the setup used for validation of RoF data transmission over PM-ERCF. We spatially multiplex four RF signals simultaneously over PM-ERCF. Each channel is detected separately. No MIMO processing is performed on modes or polarizations. This is achievable due to the minimal crosstalk in fiber propagation. The setup is shown in Fig. 5.3. In section 5.4.1, we describe the signal generation; in section 5.4.2, we briefly describe the SDM link including fiber, mode multiplexer and demultiplexer. In section 5.4.3, we describe the signal reception and overview the DSP blocks at the single-mode receiver.

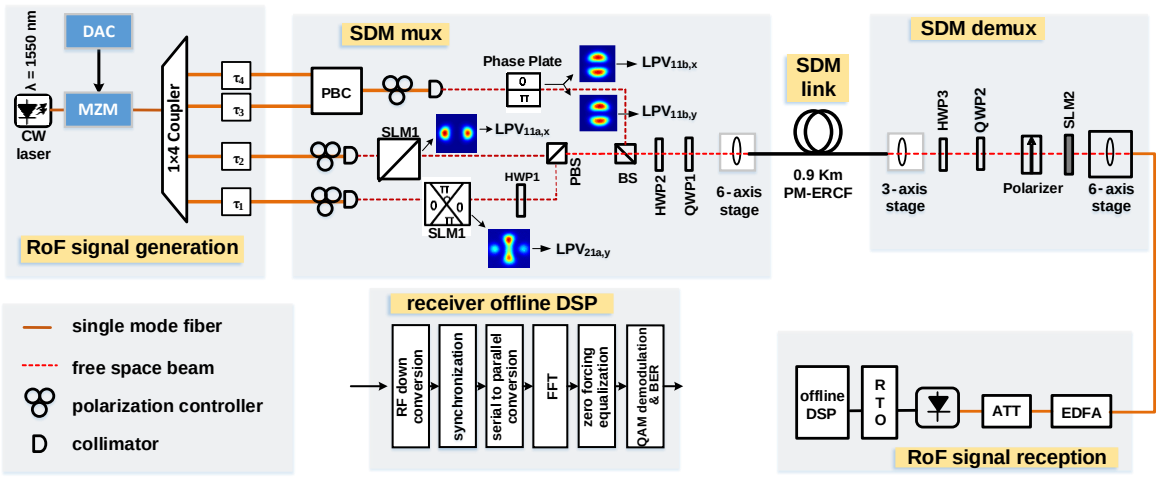

Fig. 5.3. RoF over PM-ERCF data transmission setup

5.4.1. RoF signal generation

The baseband OFDM signal is generated offline and loaded into a digital to analog converter (DAC). The OFDM signal was generated with a size 64 fast Fourier transform (FFT). There are 40 data-carrying subcarriers; the sampling rate is 640 Msample/s. The baseband OFDM signal has bandwidth of 400 MHz, with subcarrier spacing of 10 MHz. The cyclic prefix ratio of an OFDM symbol is ¼; a frame of 20 symbols has a two symbol training sequence for channel estimation. Subcarriers are modulated with 16QAM, yielding 1.152 Gbps per spatial channel. The baseband OFDM signal is up-converted to an RF carrier in DSP. The OFDM signal on the RF carrier is generated by a DAC operating at 64 Gsample/s.

The RF electrical signal is fed to a Mach-Zehnder modulator (MZM) modulating a continuous wave (CW) laser diode working at λ = 1550 nm with 100 kHz linewidth. After amplification with an erbium-doped fiber amplifier (EDFA), the optical signal carrying RoF transmissions is sent to the fiber link where four decorrelated replicas of the RoF signals are generated using an optical splitter and delay lines.

5.4.2. SDM link

The SDM link consists of a mode multiplexer, PM-ERCF and a mode demultiplexer. To generate the two polarizations of LPV_{11b}, two decorrelated signals are combined on orthogonal polarizations states of a single mode fiber (SMF) using a polarization beam combiner (PBC). A fiber polarization controller is present to insure that orthogonal linear polarization states will be present at the SMF output. The conversion to the LPV_{11b} is achieved in free space with a phase plate. We generate $LPV_{11a,x}$ and $LPV_{21a,y}$ modes with two phase masks on separately programmed sections of a spatial light modulator (SLM). The mode profile for all the generated LPV modes are shown as insets in Fig. 5.3. All free-space signals are carefully aligned in the multiplexing stage. The six axis translation stage is used to align the beams on the proper axis of the elliptically shaped ring core of the fiber. After propagation over 900 m of the PM-ERCF, light is sent to the demultiplexer. The structure of mode demultiplexer is exactly the same as one used in coherent detection. We detect one LPV mode at a time in the round-robin fashion described in section 5.3.

5.4.3. Signal Reception

After fiber transmission and mode demultiplexing, the optical signal is amplified by an EDFA and converted to the electrical domain by a 10 GHz bandwidth Agilent photodetector. The RF signal at the output of the photodetector is captured by a 80 Gsample⁄s Keysight real-time oscilloscope. The DSP is applied offline. The blocks used in DSP of the receiver include RF down conversion, low pass filtering, synchronization, serial to parallel conversion, FFT, one-tap zero-forcing equalization with one sample per symbol and 10 MHz spacing between taps, QAM demodulation and finally bit error rate (BER) measurement.

5.4.5. Crosstalk measurement for RoF experiment

The main limiting impairment of the fiber transmission is the crosstalk on each channel due to the other propagating channels. In this section, we will first characterize the crosstalk between the channels as a function of RF carrier frequencies for a range from 800 MHz to

6 GHz. We begin with RoF signals generated for data transmission in the setup described in Section II. We do the crosstalk measurement exactly with the same procedure described for coherent detection in section 5.3.1.

We observed some power fluctuations at demultiplexer output port, (around 2 dB), similar to observations discussed in [92]. In our crosstalk calculations throughout the paper, the averaged value for the received power fluctuations is considered. We sweep RF carrier frequencies from 800 MHz to 6 GHz, but the RoF signal has a consistent bandwidth of 400 MHz. Results are reported in Fig. 5.4. for case of sending all the channels simultaneously. The crosstalk is approximately -12 dB, and varies by less than one dB across channels. Our measurements show that the crosstalk on a channel changes a little over this RF carrier range, with variations of a fraction of a dB. Therefore, we restrict BER performance evaluation to only two carriers in this range– those most likely to be adopted, i.e., 2.4 GHz and 3.3 GHz.

For a better insight to the dynamics of modal interactions, we also report the crosstalk on each channel due to each of the other channels at RF carrier of 3.3 GHz in Table 5.3. The measured powers are all normalized to the power when sending and receiving $LPV_{11a,x}$ channel. For each channel, we observe the highest crosstalk from the channel that has the closest effective index to the main channel.

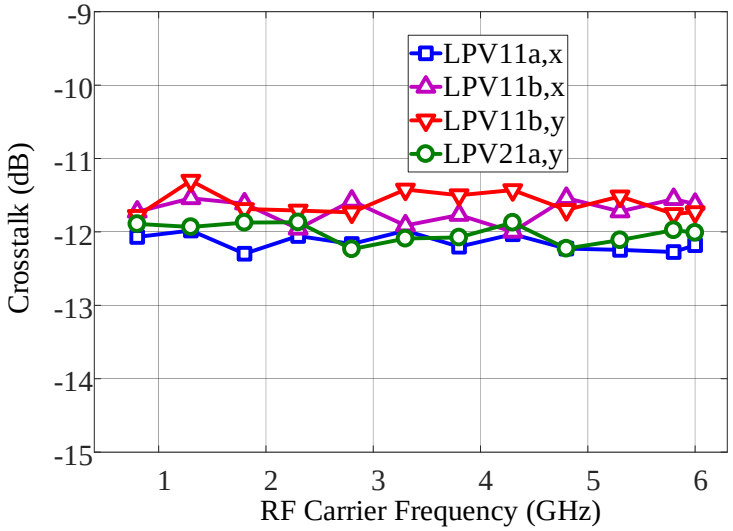

Fig. 5.4. Crosstalk versus RF carrier frequency for each mode channel

Table 5.3. Received modal power matrix at RF carrier of 3.3 GHz for bending radius of 4.5 cm in (dB); columns are transmitted modes and rows are received modes

	$LPV_{11a,x}$	$LPV_{11b,x}$	$LPV_{11b,y}$	$LPV_{21a,y}$	Total crosstalk
$LPV_{11a,x}$	0	-13.3	-19.2	-15.9	-12
$LPV_{11b,x}$	-16.5	-0.5	-15.4	-15	-11.8
$LPV_{11b,y}$	-23.8	-16.3	-1.3	-9.1	-11.6
$LPV_{21a,y}$	-19.4	-19.2	-12.3	-1.9	-11.9

5.4.6. BER Evaluation in RoF experiment

For BER evaluation in RoF experiment, we captured data in 30 sets of 10^6 samples of received signal in each of data points. We then calculated the averaged BER among all these sets. The reason for capturing 30 sets was the fluctuations observed in received power of channels. By averaging over 30 sets, we reduced the variance in our estimate of the BER, bringing it in line with other measurements in the thesis.

In Fig. 5.5 and 5.6, we report BER versus received power for RF carrier frequencies of 2.4 GHz and 3.3 GHz, respectively. As can be observed, we could reach BER below the forward error correction (FEC) threshold of 3.8×10^{-3} for all the channels. For the purpose of comparison, BER performance of back to back (B2B) and single channel data transmission are also plotted. By comparing the cases where a single channel was launched as opposed to all channels being transmitted, we observe power penalties near to 4 dB at

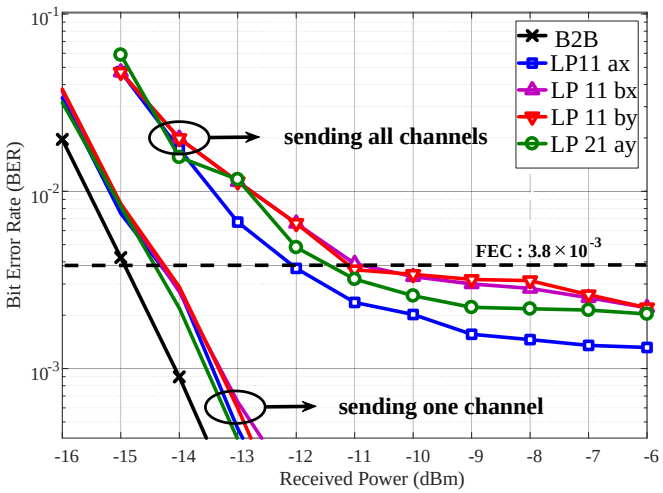

Fig. 5.5. BER versus received power at RF carrier of 2.4 GHz

the FEC threshold in case of using four channels. This penalty is mainly due to the crosstalk between channels and we will investigate it with more details in next figure.

The same trend can be observed in RF carrier of 3.3 GHz in Fig. 5.5. Referring to Fig. 5.4, we observed almost the same level of crosstalk on channels for carriers of 2.4 and 3.3 GHz and then in Fig. 5.5 and 5.6, the same BER performance.

In Fig. 5.7, we show the BER versus received power for different number of channels where the crosstalk level is different in each case. This helps us to identify the impact of crosstalk in PM-ERCF on RoF system performance and how increasing the crosstalk will impose power penalty to reach the BER of 3.8×10^{-3}. The demux is opted for reception of $LPV_{11b,y}$. BER curves are plotted for cases of sending, one, two or three channels along with the main channel of $LPV_{11b,y}$ resulting in different levels of crosstalk. The crosstalk due to each of the 3 other channels could be read from Table 5.3. For case of two channels, we transmitted the opposite polarization of the same mode, i.e. $LPV_{11b,x}$ which has the highest level of crosstalk with its effective index be the closest to $LPV_{11b,y}$. For the case of sending three channels, we examined the two cases of transmission of either $LPV_{11a,x}$ or $LPV_{21a,y}$ along with $LPV_{11b,x,y}$. Between the two other channels, the crosstalk from $LPV_{21a,y}$ which is at the same polarization of y is larger than $LPV_{11a,x}$ from the opposite polarization.

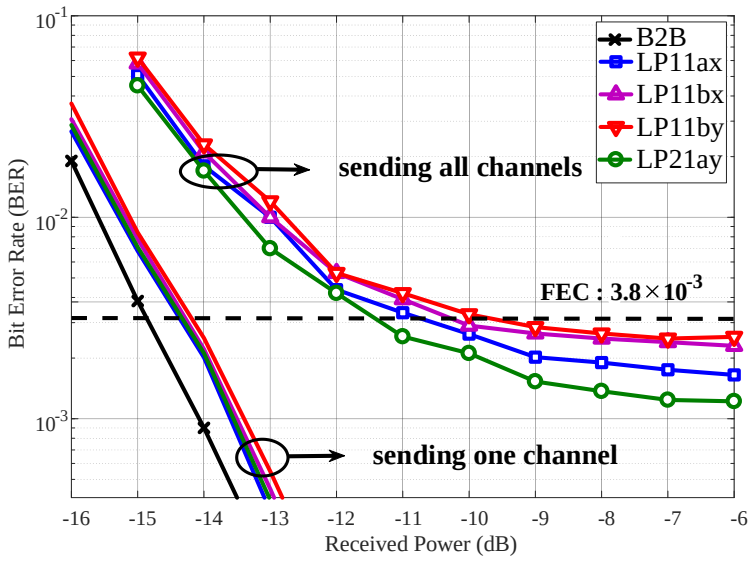

Fig. 5.6. BER versus received power at RF carrier of 3.3 GHz

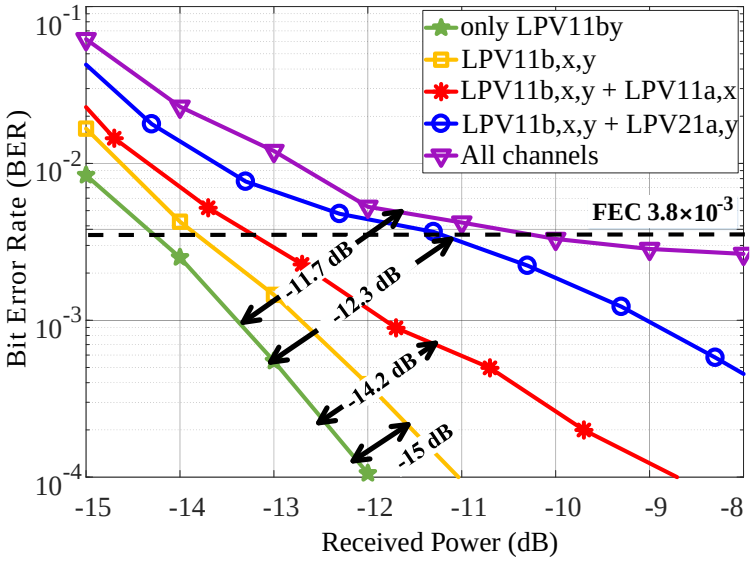

Fig. 5.7. BER versus received power at RF carrier of 3.3 GHz for $LPV11_{b,y}$ channel when transmitting various combinations of channels; insets are measured crosstalk on $LPV11_{b,y}$

The total crosstalk on $LPV_{11b,y}$ is shown for each case in Fig. 5.7 on the curves. By using the results in Fig. 5.7, we can clearly confirm that the power penalty observed in Fig. 5.5 is due to the crosstalk where higher levels of crosstalk result in higher power penalty at FEC threshold. Increase of crosstalk also increases the minimum achievable BER by system.

5.5. Comparison of ROF (direct detection) and Wideband QAM (coherent detection)

We would like also to compare the BER results of RoF in Fig. 5.5 and 5.6 with the results of coherent detection scheme in Fig. 5.2. In coherent detection, we used all the 6 channels of $LPV_{11,ax,y}$, $LPV_{11,bx,y}$ and $LPV_{21,ax,y}$ modes. With modulation format of QPSK, and for baud rates of 24 Gbaud, we could reach BERs below the FEC threshold for all the 6 channels. Therefore, at a higher crosstalk of around -9 to -10.5 dB and at a higher baud rate, we could reach better performance. The spread of BER floor for the performance evaluation versus OSNR for different channels at that case was due to two main reasons: i) the crosstalk on channels was at higher values where the system BER will be more sensitive to crosstalk changes among different channels. ii) For lower BER floors, the sensitivity and fluctuations of BER to impairments such as noise and crosstalk will be higher. Possible sources of inferior performance in RoF scheme include using non-coherent detection, non-ideal optical to electrical conversion in RoF receiver and different time scales in equalizers in DSP, i.e. time resolution of milliseconds compared to nanoseconds resolution for coherent detection.

5.6. Fiber Bending

In this section, we study the bending property of our polarization maintaining elliptical core fiber. While bending is always important, this is never more true for short links, such as front-haul, with many constraints. For example, in-building fiber installations are more likely to be torturous and impose some performance penalty.

In [90], power stability and polarization maintaining property of the fiber was examined by inducing pressure and twist using a polarization controller. Stable modes with low power fluctuations were observed. Here, we would like to observe the changes in those parameters by introducing bending. All the measurement and discussions related to bending are done using the RoF scheme.

To study the bending effect on the fiber, we begin with a main spool with radius of 18 cm on which we roll 885 meters of fiber. To this default configuration, we take a final 15 meters of fiber and roll it on progressively tighter windings. All measurements are for a total of 900 m. The "no bending" configuration has all 900 m on the main spool. The three tighter windings we examine have spools of radii of 4.5, 2.5 and 1 cm for the final 15 m of fiber.

In Fig. 5.8, we use dual y-axes to show the changes in demultiplexer output power and crosstalk. The x-axis is scaled for fiber radius, with "no bending" on the left, and more severe bending on the right. A curve is presented for each of the four channels examined. Comparing the channel power loss, $LPV_{21a,y}$ mode is clearly more sensitive to bending and has more loss than the other three channels. As a higher order mode, $LPV_{21a,y}$ has more tendency for power leakage to the cladding (or for that matter to lower order modes) and therefore more loss due to bending. Losses for the three other modes (the LPV_{11} mode group) saturate with bending to the values around -19 dB level. The higher mode has 8 dB more loss at the same bending radius.

The crosstalk level increases with decreasing the bending radius for all modes. We see an almost linear progression of crosstalk in dB for tight windings. These crosstalk levels are enough to push the system into a region where MIMO processing is required, indicating that bending is a serious concern.

The measurements in Fig. 5.8 are done at RF carrier of 2.4 GHz. To study the impact of RF carrier frequency on crosstalk values when bending occurs, we swept the RF carrier frequency from 800 MHz to 6 GHz. The results for bending radius of 4.5 cm are depicted in Fig. 5.9. For the purpose of comparison, the crosstalk levels for no bending case is also shown. As can be observed, the bending induced crosstalk levels, similar to the case of no bending, are almost independent of RF carrier frequency; however, due to dynamics of modal interactions due to bending, the difference among crosstalk on the four channels is larger than the case of no bending. For a better insight to dynamics of modal mixing, we also report, in Table 5.4., the received modal powers at RF carrier of 3.3 GHz at bending radius of 4.5 cm. Again, the powers are all normalized to the received power when sending and receiving $LPV_{11a,x}$. By comparing the received powers in tables 5.2 and 5.4, we observe

the highest crosstalk increase on channels is contributed by $LPV_{21,a,y}$ mode. This is due to higher tendency of higher order modes for power leakage to lower order modes. It

Table 5.4. Received modal power matrix at RF carrier of 3.3 GHz for bending radius of 4.5 cm in (dB); columns are transmitted modes and rows are received modes

	$LPV_{11a,x}$	$LPV_{11b,x}$	$LPV_{11b,y}$	$LPV_{21a,y}$	Total crosstalk
$LPV_{11a,x}$	0	-13.3	-19.2	-15.9	-10.3
$LPV_{11b,x}$	-16.5	-0.5	-15.4	-15	-6.1
$LPV_{11b,y}$	-23.8	-16.3	-1.3	-9.1	-8.3
$LPV_{21a,y}$	-19.4	-19.2	-12.3	-1.9	-10.1

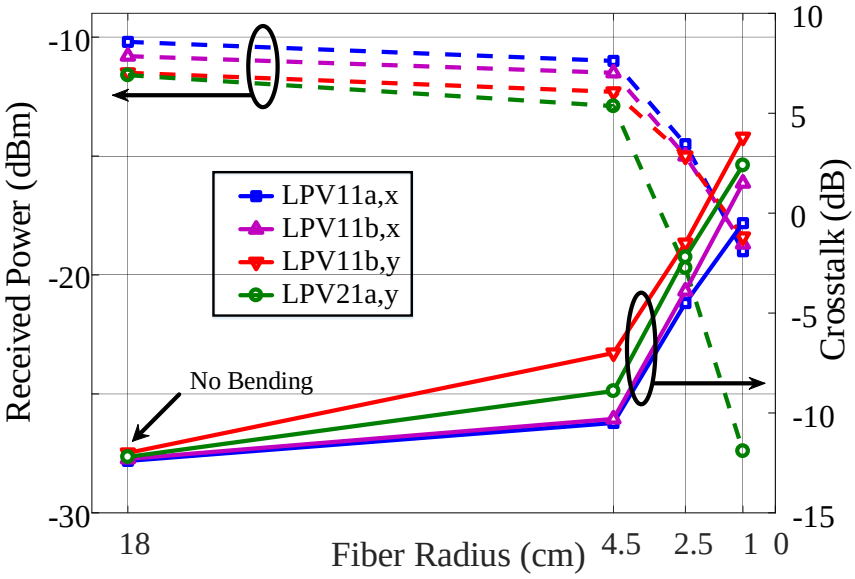

Fig. 5.8. Loss and crosstalk measurement versus fiber spool bending at RF carrier of 2.4 GHz

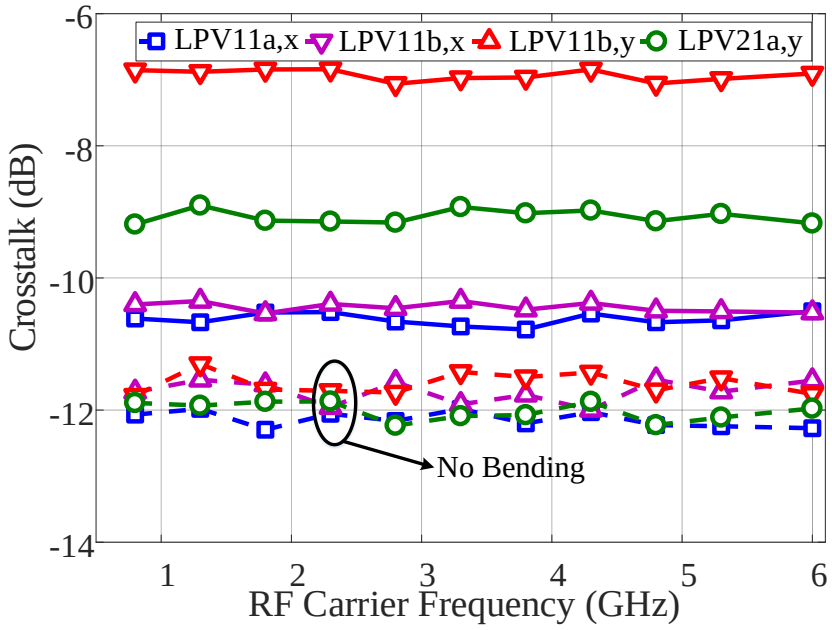

Fig. 5.9. Crosstalk on channels versus RF carrier frequency with bending fiber of radius 4.5 cm added to the main spool

has the highest interaction with $LPV_{11,b,y}$ whose effective index is closest to $LPV_{21,a,y}$ and they are both on polarization *y*.

Although the bending results in increase of crosstalk between channels but the two polarizations of LPV_{11b} mode remain well separated. This confirms the coupling between orthogonal polarizations is resistant against bending. The crosstalk levels of –15.5, –14.8, -14 and -13.1 dB from $LPV_{11,b,y}$ on $LPV_{11,b,x}$ channel is observed in cases of no bending and bending spools with radiuses of 4.5, 2.5 and 1 cm, respectively. In Fig. 5.10, the BER performance for case of sending $LPV_{11bx,y}$ and receiving LPV_{11bx} at RF carrier of 2.4 GHz is plotted. The RF signal could be recovered; at the FEC threshold, a maximum power penalty of around 2 dB is observed. This signifies that, even under severe bending conditions, PM-ERCF fiber can provide at least two channels without considerable power penalty and without recourse to MIMO processing to compensate for impairments in optical channel.

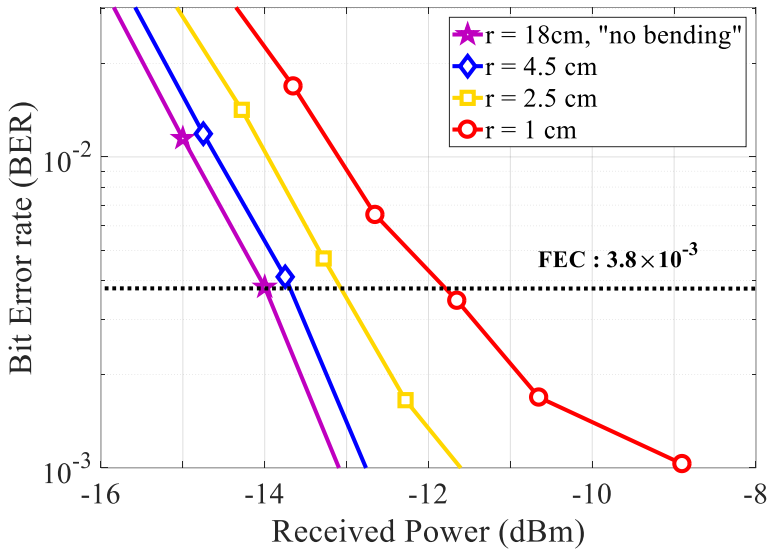

Fig. 5.10. BER vs received power for sending two polarizations of LPV11b with bending applied to the fiber at RF carrier of 2.4 GHz

5.7. Conclusion

We showed for the first time, transmission of four RF signals over four LPV modes in a PM-ERCF via spatial division multiplexing with a total bit rate of 4.608 Gbps. Successful transmission on RF carriers of 2.4 GHz and 3.3 GHz was demonstrated without using MIMO processing. The fiber crosstalk could impose 3-4 dB of power penalty at the 3.8×10^{-3} FEC threshold. In investigating crosstalk changes due to the bending, we showed two polarizations of a mode remain separated under bending, where data on polarization states could be recovered without recourse to MIMO processing.

Furthermore, we demonstrated, for the first time, MIMO-free transmission of six QPSK data channels over six vector modes of PM-ERCF. The power penalty of around 8 dB was observed for switching from sending only one channel to case of sending six channels.

Chapter 6

Conclusions and Future Work

In this thesis, we studied two aspects of data transmission and channel characterization for short reach MDM systems using specialty designed fibers in our group. Our data transmission experiments included both coherent and non-coherent experiments.

Our first contribution was to demonstrate for the first time, data transmission using four channels in OAM modes of order zero and one over 1.4 km of RCF fiber. Former demonstrations either did not use polarization multiplexing, or if PDM was used, then optical polarization demultiplexing was used, i.e., polarization controllers. We introduced a new mode demultiplexer setup where we had access to all the channels at the output of mode demultiplexer simultaneously. This mode demultiplexer enabled us to use electrical polarization demultiplexing in DSP instead of optical demultiplexing. The DSP blocks used in our transmission experiments were the standard DSP blocks in dual polarization single mode coherent detection systems proving the compatibility of the new fibers with the already available DSP in terms of the required functional blocks. Since design of integrated mode multiplexer and demultiplexer is still a topic of research, using our free space optics mode multiplexer and demultiplexer setup, we investigated how imperfect mode

demultiplexer can affect the performance of MDM system. We also demonstated we could reach as high as 256 Gbps over a single wavelength for this fiber.

In our second contribution, we studied the modal interactions in OAM fibers. Since an analytical model describing the channel and modal impairment is not available yet, we experimentally characterized and investigated the modal interactions that could affect the system performance and complexity. We showed, for the first time, the impact of two parasitic modes of TE_{01} and TM_{01} and how their interaction with HE_{21} mode carrying $OAM_{\pm1}$ channels can result in increased equalizer memory depth. By using time-of-flight and channel impulse response measurements, we showed the interactions of TE_{01} and TM_{01} with data carrying HE_{21} mode results in pulse broadening in the received data. As a solution, we suggest using higher order OAM modes instead of using modes of order one.

In our third contribution, we probed the feasibility of using mode multiplexing in a non-coherent scheme over a specially-designed polarization maintaining fiber for vector mode propagation. The radio over fiber system with non-coherent detection was chosen because of the huge interest and investment in 5G systems. 5G systems require multiple stream transmission and capacity increase in front haul systems. For this application, we successfully demonstrated data transmission over four vector modes at two RF carriers of 2.4 and 3.3 GHz for WiFi and 5G systems. We also characterized the crosstalk, the main modal impairment in non-coherent systems, for different RF frequency bands. We showed that our fiber performance is almost insensitive to change of RF carrier for frequencies ranging from 800 MHz to 6 GHz. We also showed how different levels of crosstalk impact system performance in non-coherent RoF systems. We investigated the bending characteristics and polarization maintaining property of our fiber; we showed via characterization and data transmission, even under severe bending, the data in two polarizations of a mode could be recovered with power penalty of around 2 dB.

For the future research, there are different directions and aspects of MDM systems that could be studied. Here, we briefly review them:

- An analytical or semi-analytical model for modal interaction for weak mode coupling regime would be useful for studying the impairments versus fiber and MDM link parameters.

- For MDM systems, fiber design is the most crucial part and there is still a lot of opportunities for improved designs. New fiber designs with lower modal mixing over longer distances or among higher number of modes are very interesting.

- For OAM-MDM systems, we used modes of order zero and one and we discussed the challenges in using modes of order one. Fibers that could support higher order OAM modes can be studied in future.

- Another aspect of MDM systems is the design of integrated mode multiplexer and demultiplexer. In this thesis, we were using free space optics components to build our mode multiplexer and demultiplexer. The alignment procedure for the free space optics is time consuming and unstable over time. An integrated solution will be highly desirable and helpful in terms of time efficiency for experimental studies. Techniques or approaches that could result in low modal mixing in mode multiplexer and demultiplexer will also enhance the performance of MDM system.

- We used QPSK modulation format in our data transmission with coherent detection. Possibility of using higher order modulations formats versus different lengths of fibers and comparing with the QPSK as the baseline can be done in future.

- In this thesis, we always were using wavelength of 1550 nm. Studying the performance of these specialty fibers or new fibers over different frequency bands could be another aspect for future studies. Running WDM-MDM or super-channel-

MDM experiments where multiplexing in both dimensions of wavelength and space are exploited will be interesting for demonstration purposes.

Publication List

[1] Reza Mirzaei Nejad, Karen Allahverdyan, Pravin Vaity, Siamak Amiralizadeh, Charles Brunet, Younès Messaddeq, Sophie LaRochelle and Leslie A. Rusch, "Orbital Angular Momentum Mode Division Multiplexing over 1.4 km RCF Fiber," in Proc. Conf. Laser Opt. elec. (CLEO) 2016, Paper SW4F.3.

[2] Reza Mirzaei Nejad, Karen Allahverdyan, Pravin Vaity, Siamak Amiralizadeh, Charles Brunet, Younès Messaddeq, Sophie LaRochelle, and Leslie A. Rusch, , "Mode Division Multiplexing Using Orbital Angular Momentum Modes Over 1.4-km Ring Core Fiber," Journal of Lightwave Technology, vol. 34, no. 18, Sept. 2016.

[3] Reza Mirzaei Nejad, K. Allahverdyan, C. Brunet, S. LaRochelle and L. A. Rusch, "Experimental Study of Receiver Complexity in OAM-MDM Transmission Systems," 2016 IEEE Photonics Conference (IPC), Waikoloa, 2016, TuB2.4.

[4] Reza Mirzaei Nejad, L. Wang, J. Lin, S. LaRochelle, L. A. Rusch, "Parasitic Effect of TE and TM modes in OAM-MDM Transmission Systems," in Proc. Conf. Laser and Electro-Optics (CLEO), San Jose, CA, 2017, SW4I.2.

[5] Reza Mirzaei Nejad, Lixian Wang, Jiachuan Lin, Sophie LaRochelle, and Leslie A. Rusch, , "The impact of Modal Impairments on Receiver Complexity in OAM Fibers," Journal of Lightwave Technology, vol. 35, no. 21, Nov. 2017.

[6] Lixian Wang, Reza M. Nejad, A. Corsi, J. Lin, Y. Messaddeq, L. A. Rusch and S. LaRochelle, "MIMO-Free Transmission over Six Vector Modes in a Polarization Maintaining Elliptical Ring Core Fiber," OFC 2017.

[7] Lixian Wang, Reza Mirzaei Nejad, Alessandro Corsi, Jiachuan Lin, Younès Messaddeq, Leslie Rusch, Sophie LaRochelle, "Linearly polarized vector modes: enabling MIMO-free mode-division multiplexing", Optics Express, vol. 25, no.10, pp. 11736-11748, May 2017.

[8] Reza Mirzaei Nejad, Farzan Tavakoli, Lixian Wang, Xun Guan, Sophie Larochelle, and Leslie A. Rusch, "Four-Channel RoF Transmission over Polarization maintaining Elliptical Ring Core Fiber," Submitted to OFC 2018.

[9] Reza Mirzaei Nejad, Farzan Tavakoli, Lixian Wang, Xun Guan, Sophie Larochelle, and Leslie A. Rusch, "RoF Data Transmission over Polarization Maintaining Few Mode Elliptical Core Fiber," submitted to Journal of Lightwave Technology.

[10] Reza Mirzaei Nejad, Leslie A. Rusch, Jawad A. Salehi, "Two Stage Code Acquisition in Wireless Optical CDMA Communications using Optical Orthogonal Codes," IEEE Transactions on Communications, vol.64, no.8, Aug. 2016.

Bibliography

[1] R.W. Tkach, Scaling optical communications for the next decade and beyond, Bell Labs Tech. J. 14 (4) (2010) 3–9.

[2] S.K. Korotky, Traffic trends: drivers and measures of cost-effective and energy-efficient technologies and architectures for backbone optical networks, in: Proc. OFC, OM2G.1, 2012.

[3] J. Gray, P. Shenoy, Rules of thumb in data engineering, Microsoft Research Technical Report MS-TR-99-100, 2000.

[4] J.G. Apostolopoulos et al., The road to immersive communication, Proc. IEEE 100 (4) (2012) 974–990.

[5] H. Kogelnik, On optical communication: Reflections and perspectives, Proc. ECOC (2004) Mo1.1.1.

[6] J. Renaudier et al., Spectrally efficient long-haul transmission of 22-Tb/s using 40-Gbaud PDM-16QAM with coherent detection, in: Proc. OFC, 2012, OW4C.2.

[7] G. Raybon et al., 1-Tb/s dual-carrier 80-GBaud PDM-16QAM WDM transmission at 5.2 b/s/Hz over 3200 km, in: Proc. IPC, 2012, PD1.2.

[8] S. Chandrasekhar, X. Liu, OFDM based superchannel transmission technology, J. Lightwave Technol. 30 (24) (2012) 3816–3823.

[9] D. Qian et al., "101.7-Tb/s (370x294-Gb/s) PDM-128QAM-OFDM transmission over 3 × 55-km SSMF using pilot-based phase noise mitigation," in: Proc. OFC, , 2011, PDPB5.

[10] R.-J. Essiambre, G. Kramer, P. J. Winzer, G. J. Foschini, and B. Goebel, "Capacity limits of optical fiber networks," J. Lightw. Tech., vol. 28, no. 4, pp. 662–701, Feb. 2010.

[11] Ivan Kaminow, Tingye Li, Alan Willner, Optical Fiber Telecommunications VI-B, 6th Edition, Academic Press, 2013.

[12] W. Mohammed, M. Pitchumani, A. Mehta, and E. G. Johnson, "Selective excitation of the LP mode in step index fiber using a phase mask," Opt. Eng., vol. 45, no. 7, pp. 74602-1–74602-7, 2006.

[13] Daniel Flamm, Christian Schulze, Darryl Naidoo, Siegmund Schröter, Andrew Forbes, and Michael Duparré "All-Digital Holographic Tool for Mode Excitation and Analysis in Optical Fibers," J. Of Lightw. Tech., vol. 31, no. 7, Apr. 2013.

[14] T. A. Birks, I. Gris-Sánchez,1 S. Yerolatsitis, S. G. Leon-Saval, and R. R. Thomson, "The photonic lantern," Advances in Optics and Photonics, vol.7, no. 2, pp.107-167, 2015.

[15] Pierre Sillard, Marianne Bigot-Astruc, and Denis Molin, "Few-Mode Fibers for Mode-Division-Multiplexed Systems," J. Of Lightw. Tech., vol. 32, no. 16, Aug, 2014.

[16] Q. Kang et al. "Modal gain control in a multimode erbium doped fiber amplifier incorporating ring doping," ECOC 2012, P1.05.

[17] Seb J. Savory, "Digital filters for coherent optical receivers," OPT. EXP., vol. 16, no. 2 , pp.804-817, Jan. 2008.

[18] S. Randel , R. Ryf , A. H. Gnauck , M. A. Mestre , C. Schmidt , R.-J. Essiambre , P. J. Winzer , R. Delbue , P. Pupalaikis , A. Sureka , Y. Sun , X. Jiang , R. Lingle, Jr. "Mode-Multiplexed 6×20-GBd QPSK Transmission over 1200-km DGD-Compensated Few-Mode Fiber", OFC/NFOEC Postdeadline Papers , 2012, PDP5C.5

[19] Nicolas K. Fontaine, Roland Ryf, Haoshuo Chen, Amado Velazquez Benitez, J. E. Antonio Lopez, R. Amezcua Correa, Binbin Guan, Burcu Ercan, Ryan P. Scott, S. J. Ben Yoo, Lars Gruner-Nielsen, Yi Sun, and Robert J. Lingle, "30×30 MIMO transmission over 15 spatial modes," in Proc. Opt. Fiber Commun. Conf. (OFC) 2015, Postdeadline Paper Th5C.1.

[20] M.G. Taylor, Algorithms for coherent detection, in: Proc. OFC, OThL4, 2010.

[21] J.G. Proakis, M. Salehi “Digital Communications,” 5th edition, McGrew Hill inc., NY, 2008.

[22] Irshaad Fatadin, David Ives, and Seb J. Savory, “Blind Equalization and Carrier Phase Recovery in a 16-QAM Optical Coherent System,” *J. Lightw. Technol.,* vol. 27, no. 15, pp.3042-3049, Aug, 2009.

[23] Kazuro Kikuchi, “Fundamentals of Coherent Optical Fiber Communications,” *J. Lightw Technol,* vol. 34, no. 1, pp.157-179, Jan 2016.

[24] D. J. Richardson, J. M. Fini, and L. E. Nelson, “Space-division multiplexing in optical fibers,” *Nat. Photon.*, vol. 7, pp. 354–362, May 2013.

[25] K.-P. Ho and J. M. Kahn, “Linear propagation effects in mode-division multiplexing systems,” *J. Lightw. Technol.*, vol. 32, no. 4, pp. 614–628, Feb. 2014.

[26] N. Fontaine, “Devices and components for space-division multiplexing in few-mode fibers,” in *Proc. Opt. Fiber Commun. Conf. (OFC)* 2013, Paper OTh1B.3.

[27] R. Ryf, S. Randel, A. H. Gnauck, C. Bolle, A. Sierra, S. Mumtaz, M. Esmaeelpour, E. C. Burrows, R-J. Essiambre, P. J. Winzer, D. Peckham, A. McCurdy, and R. Lingle, “Mode-division multiplexing over 96 km of few-mode fiber using coherent 6×6 MIMO processing,” *J. Lightw. Technol.*, vol. 30, no. 4, pp. 521–531, Feb. 2012.

[28] N. K. Fontaine, R. Ryf, H. Chen, A. V. Benitez, B. Guan, R. Scott, B. Ercan, S. J. B. Yoo, L. E. Grüner-Nielsen, Y. Sun, R. Lingle, E. Antonio-Lopez, and R. Amezcua-Correa, “30×30 MIMO transmission over 15 spatial modes,” in *Proc. Opt. Fiber Commun. Conf. (OFC)* 2015, *Postdeadline Paper* Th5C.1.

[29] R. Ryf, H. Chen, N. K. Fontaine, A. M. Velazquez-Benitez, Jose Antonio-Lopez, C. Jin, B. Huang, M. Bigot-Astruc, D. Molin, F. Achten, P. Sillard, R. Amezcua-Correa, “10-Mode mode-multiplexed transmission over 125-km single-span multimode fiber,” in *Proc. Eur. Conf. Opt. Commun. (ECOC)*, 2015.

[30] Feng Feng, Xuhan Guo, George S. D. Gordon, X. Q. Jin, F. P. Payne, Y. Jung, Q. Kang, S. Alam, P. Barua, J. K. Sahu, D. J. Richardson, Ian H. White, Timothy D. Wilkinson, “All-optical Mode-Group Division Multiplexing Over a Graded-Index Ring-Core Fiber with Single Radial Mode,” in Proc. Opt. Fiber Commun. Conf. (OFC) 2016, Paper W3D.5.

[31] D. Andrews, "Orbital Angular Momentum in Quantum Communication and Information" in *Structured Light and Its Applications, 1st ed.,* New York: Academic Press, 2008, pp.271-291.

[32] Nenad Bozinovic, Steven Golowich, Poul Kristensen and Siddharth Ramachandran, "Control of orbital angular momentum of light, with optical fibers," *Opt. Lett.,* vol. 37, no. 13, pp.2451-2453, Jul. 2012.

[33] Nenad Bozinovic, Poul Kristensen, Siddharth Ramachandran "Long-range fiber-transmission of photons with orbital angular momentum", in *Proc. Conf. Laser Opt. elec.* (CLEO) 2011, Paper CTuB1.

[34] Siddharth Ramachandran, et al, "Generation and propagation of radially polarized beams in optical fibers", *Opt. Lett.,* vol. 34, no. 16, pp. 2525-252, Aug. 2009.

[35] N. Bozinovic, Y. Yue, Y. Ren, M. Tur, P. Kristensen, A. Willner, and S. Ramachandran, "Orbital Angular Momentum (OAM) based Mode Division Multiplexing (MDM) over a km-length Fiber," in *Proc. Eur. Conf. Opt. Commun. (ECOC),2012, Postdeadline Paper* Th.3.C.6.

[36] N. Bozinovic, Y. Yue, Y. Ren, M. Tur, P. Kristensen, H. Huang, A. E. Willner, S. Ramachandran, "Terabit-Scale Orbital Angular Momentum Mode Division Multiplexing in Fibers," *Science,* vol. 340, pp. 1545-1548, Jun. 2013.

[37] Joel Carpenter , Benn C. Thomsen , Timothy D. Wilkinson, "Optical vortex based Mode Division Multiplexing over graded-index multimode fibre,"in Proc. Opt. Fiber Commun. Conf. (OFC) 2013, Paper OTh4G.3.

[38] Joel Carpenter, Benn C. Thomsen, and Timothy D. Wilkinson, "Degenerate Mode-Group Division Multiplexing," J. Lightw. Technol., vol. 30, no. 24, pp. 3946-3952, Dec. 2012.

[39] S. Golowich, "Asymptotic theory of strong spin-orbit coupling in optical fiber," *Opt. Lett.,* vol.39, no.1, pp. 92-95, Jan. 2014.

[40] Roland Ryf, S. Randel, A. H. Gnauck, C. Bolle, A. Sierra, S. Mumtaz, M. Esmaeelpour, E. C. Burrows, R-J. Essiambre, P. J. Winzer, D. Peckham, A. McCurdy,

and R. Lingle, “Mode-division multiplexing over 96 km of few-mode fiber using coherent 6×6 MIMO processing*,” J. Lightw. Technol.*, vol. 30, no. 4, pp. 521–531, Feb. 2012.

[41] Nenad Bozinovic, Y. Yue, Y. Ren, M. Tur, P. Kristensen, H. Huang, A. E. Willner, S. Ramachandran, “Terabit-Scale Orbital Angular Momentum Mode Division Multiplexing in Fibers,” *Science*, vol. 340, pp. 1545-1548, Jun. 2013.

[42] Long Zhu, A. Wang, S. Chen, J. Liu, C. Du, Q. Mo and J. Wang, “Experimental Demonstration of Orbital Angular Momentum (OAM) Modes Transmission in a 2.6 km Conventional Graded-Index Multimode Fiber Assisted by High Efficient Mode-Group Excitation,” *in Proc. Opt. Fiber Commun. Conf.* (OFC) 2016, W2A.32.

[43] Joel Carpenter, B. C. Thomsen, and T. D. Wilkinson, “Degenerate Mode-Group Division Multiplexing,” *J. Lightw. Technol.*, vol. 30, no. 24, pp. 3946-3952, Dec. 2012.

[44] Giovanni Milione, H. Huang, M. P. J. Lavery, T. A. Nguyen, G. Xie, Y. Cao, M. Willner, M. Tur, S. Dolinar, R. R. Alfano, M. J. Padgett, and A. E. Willner, “Orbital-Angular-Momentum Mode (De)Multiplexer: A Single Optical Element for MIMO-based and non-MIMObased Multimode Fiber Systems,” *in Proc. Opt. Fiber Commun. Conf.* (OFC) 2014, M3K.6.

[45] Jun Liu, S. Li, Y. Ding, A. Wang, L. Zhu, S. Li, S. Zheng, S. Chen, S. Yu, X. Cai, and J. Wang, “Demonstration of Orbital Angular Momentum (OAM) Modes Emission from a Silicon Photonic Integrated Device for 20 Gbit/s QPSK Carrying Data Transmission in Few-Mode Fiber,” *in Proc. Conf. Laser and Electro-Optics* (CLEO) 2016, JTh2A.129.

[46] Nicolas K. Fontaine, R. Ryf, H. Chen, A. V. Benitez, B. Guan, R. Scott, B. Ercan, S. J. B. Yoo, L. E. Grüner-Nielsen, Y. Sun, R. Lingle, E. Antonio-Lopez, and R. Amezcua-Correa, “30×30 MIMO transmission over 15 spatial modes,” in *Proc. Opt. Fiber Commun. Conf.* (OFC) 2015, Postdeadline Paper, Th5C.1.

[47] Roland Ryf, H. Chen, N. K. Fontaine, A. M. Velazquez-Benitez, José Antonio-Lopez, C. Jin, B. Huang, M. Bigot-Astruc, D. Molin, F. Achten, P. Sillard, R. Amezcua-Correa, “10-Mode mode-multiplexed transmission over 125-km single-span multimode fiber,” in *Proc. Eur. Conf. Opt. Commun*. (ECOC), 2015.

[48] Philippe Genevaux, C. Simonneau, G. Labroille, B. Denolle, O. Pinel, P. Jian, J.-F. Morizur, G. Charlet, “6-mode Spatial Multiplexer with Low Loss and High Selectivity for Transmission over Few Mode Fiber,” *in Proc. Opt. Fiber Commun. Conf.* (OFC) 2015, W1A.5.

[49] Massimiliano Salsi, Clemens Koebele, Gabriel Charlet, Sébastien Bigo, “Mode Division Multiplexed Transmission with a weakly coupled Few-Mode Fiber,” in Proc. Opt. Fiber Commun. Conf. (OFC) 2012, OTu2C.5

[50] Ezra Ip, G. Milione, Ming-Jun Li, Neda Cvijetic, Konstantinos Kanonakis, Jeffery Stone, Gaozhu Peng, Xesús Prieto, Carlos Montero, Vicente Moreno, and Jesús Liñares, “SDM transmission of real-time 10GbE traffic using commercial SFP + transceivers over 0.5km elliptical-core few-mode fiber,” *Opt. Exp.*, vol. 23, no. 13, pp. 17120-17126, Jun 2015.

[51] Ezra Ip, N. Cvijetic, G. Milione, K. Kanonakis, T. Wang, M.-J. Li, J. Stone, G. Peng, “MIMO Equalization Analysis for SDM Transmission Over 2km Elliptical-Core Few-Mode Fiber for Datacenter Applications,” *Proceedings of APCC* 2015.

[52] L. Wang, R. M. Nejad, A. Corsi, J. Lin, Y. Messaddeq, L. A. Rusch, and S. LaRochelle, "MIMO-Free Transmission over Six Vector Modes in a Polarization Maintaining Elliptical Ring Core Fiber," *in Proc. Opt. Fiber Commun. Conf.* (OFC) 2017, Tu2J.2, 2017.

[53] Nenad Bozinovic, P. Kristensen, and S. Ramachandran, “Long-range fiber-transmission of photons with orbital angular momentum”, *in Proc. Conf. Laser Opt. elec.* (*CLEO*) 2011, CTuB1.

[54] Patrick Gregg, P Kristensen, and S. Ramachandran, “13.4km OAM state propagation by recirculating fiber loop,” Opt. Exp., vol. 24, no. 17, pp. 18938-18947, Aug 2016.

[55] Reza Mirzaei Nejad, K. Allahverdyan, P. Vaity, S. Amiralizadeh, C. Brunet, Y. Messaddeq, S. LaRochelle, and L. A. Rusch, “Mode Division Multiplexing Using Orbital Angular Momentum Modes Over 1.4-km Ring Core Fiber,” *J. Lightwave Technol.*, vol. 34, no. 18, pp. 4252-4258, Sept. 2016.

[56] Kasper Ingerslev et al., “12 Mode, MIMO-Free OAM Transmission,” *in Proc. Opt. Fiber Commun. Conf. (OFC) 2017*, M2D.1.

[57] K.-P. Ho and J. M. Kahn, “Linear propagation effects in mode-division multiplexing systems,” *J. Lightw. Technol.*, vol. 32, no. 4, pp. 614–628, Feb. 2014.

[58] Xianqing Jin, A. Gomez, K. Shi, B. C. Thomsen, F. Feng, G. S. D. Gordon, T. D. Wilkinson, Y. Jung, Q. Kang, P. Barua, J. Sahu, S. Alam, D. J. Richardson, D. C. O’Brien, and F. P. Payne , “Mode Coupling Effects in Ring-Core Fibers for Space-Division Multiplexing Systems,” *J. Lightw. Technol*., vol. 34, no. 14, pp. 3365-3372, Jul. 2016.

[59] Charles Brunet, B. Ung, L Wang, Y. Messaddeq, S. LaRochelle, and L. A. Rusch, “Design of a family of ring-core fibers for OAM transmission studies,” *Opt. Exp.*, vol. 23, no. 8, pp.10553-10563, 2015.

[60] Bora Ung, P. Vaity, L. Wang, Y. Messaddeq, L. A. Rusch, and S. LaRochelle, “Few-mode fiber with inverse-parabolic graded-index profile for transmission of OAM-carrying modes,” *Opt. Exp.*, vol. 22, no. 15, pp. 18044–18055, Jul. 2014.

[61] P. Z. Dashti, F. Alhassen, and H. P. Lee, “Observation of orbital angular momentum transfer between acoustic and optical vortices in optical fiber,”Phys. Rev. Lett., vol. 96, p. 043604, Feb. 2006.

[62] Kai Shi, A. Gomez, X. Q. Jin, Y. Jung, C. Quintana, D. C. O’Brien, F. P. Payne, P. Barua, J. Sahu, Q. Kang, S.-U. Alam, D. J. Richardson, and B. C. Thomsen, “Simplified impulse response characterization for mode division multiplexed systems,” *in Proc. Opt. Fiber Commun. Conf.* (OFC) 2016, W4F.3.

[63] Seb J. Savory “Digital Coherent Optical Receivers: Algorithms and Subsystems,” *IEEE J. Sel. Topics Quantum Electron*., vol. 16, no. 5, pp. 1164-1179, Sep. 2010.

[64] Kazuro Kikuchi, “Clock recovering characteristics of adaptive finite-impulse-response filters in digital coherent optical receivers,” *Opt. Exp.*, vol. 19, no. 6, pp. 561114- 561119, Mar 2011.

[65] Randel, P. J. Winzer, M. Montoliu and R. Ryf, "Complexity analysis of adaptive frequency-domain equalization for MIMO-SDM transmission," in *Proc. Eur. Conf. Opt. Commun.* , (ECOC) 2013.

[66] Dalma Novak, Rodney B. Waterhouse, Ampalavanapillai Nirmalathas, Christina Lim, Prasanna A. Gamage, Thomas R. Clark, Jr., Michael L. Dennis, and Jeffrey A. Nanzer, "Radio-Over-Fiber Technologies for Emerging Wireless Systems," IEEE J. Quantum Electron., vol. 52, no. 1, Jan. 2016.

[67] Cisco, "Cisco Visual Networking Index: Global Mobile Data Traffic Forecast," Cisco white paper, Feb. 2017.

[68] Maria Morant, Josep Prat and Roberto Liorente, "Radio-Over-Fiber Optical Polarization-Multiplexed Networks for 3GPP Wireless Carrier-Aggregated MIMO Provision," J. Lightwave Tech., vol. 32, no. 20, pp. 3721-3727, Oct. 2014.

[69] Ze Dong, Jianjun Yu, Xinying Li, Zizheng Cao, Lin Chen, and Gee-Kung Chang, "Integration of 112-Gb/s PDM-16QAM Wireline and Wireless Data Delivery in Millimeter Wave RoF System," in Proc. Opt. Fiber Commun. Conf. (OFC) 2015, OM3D.2.

[70] Lei Deng, Xiaodan Pang, Ying Zhao, M. B. Othman, Jesper Bevensee Jensen, Darko Zibar, Xianbin Yu, Deming Liu, and Idelfonso Tafur Monroy, "2x2 MIMO-OFDM Gigabit fiber-wireless access system basedon polarization division multiplexed WDM-PON," Optics Express, vol. 20, no. 4, pp. 4369-4375, Feb. 2012.

[71] M. Kenji, T. Takayoshi, H. Takeshi, T. Katsutoshi, K. Shozo, H. Kazutaka, T. Tomohiro, K. Jun-ichi, Y. Naoto, and I. Katsumi, "Experimental demonstration of MIMO RF signal transmission in RoF-DAS over WDM-PON," in Proceedings of IEEE International Topical Meeting on & Microwave Photonics Conference, Asia-Pacific, MWP/APMP, 2011, pp. 25–28.

[72] T. Tashiro, K. Miyamoto, K. Hara, T. Taniguchi, J. Nakagawa, N. Yoshimoto, K. Iwatsuki, T. Nishiumi, T. Higashino, K. Tsukamoto, and S. Komaki, "Broadband Ubiquitous Network Based on RoF-DAS over WDM-PON," in Proc. Opt. Fiber Commun. Conf. (OFC) 2011, OWT2.

[73] George S. D. Gordon, Michael J. Crisp, Richard V. Penty, Timothy D. Wilkinson, and Ian H. White "Feasibility Demonstration of a Mode Division Multiplexed MIMO-Enabled Radio-Over-Fiber Distributed Antenna System," J. Lightwave. Tech., vol. 32, no. 20, pp-3521-3528, Oct. 2014.

[74] George Gordon, Joel Carpenter, Michael Crisp,Timothy Wilkinson,Richard Penty, Ian White, "Demonstration of Radio-over-Fibre Transmission of Broadband MIMO

over Multimode Fibre using Mode Division Multiplexing," in Proc. Eur. Conf. Opt. Commun. (ECOC), 2012.

[75] Yi Lei, Jianqiang Li, Yuting Fan, Dawei Yu, Songnian Fu, Feifei Yin, Yitang Dai, And Kun Xu, "Space-division-multiplexed transmission of 3x3 multiple-input multiple-output wireless signals over conventional graded-index multimode fiber," Optics Express, vol. 24, no. 25, pp-28372-28382, Dec. 2016.

[76] Jiale He, Borui Li, Lei Deng, Ming Tang, Lin Gan, Songnian Fu, Perry Ping Shum, and Deming Liu, "Experimental investigation of inter-core crosstalk tolerance of MIMO-OFDM/OQAM radio over multicore fiber system," Optics Express, vol. 24, no. 12, pp. 13418-13428, Jun. 2016.

[77] Andrés Macho, Maria Morant and Roberto Llorente, "Experimental Analysis of Multicore Crosstalk Impact on MIMO LTE-A Radio-over-Fibre Optical Systems," IEEE workshop on Fiber-Wireless Integrated Technologies, Systems and Networks, ICC 2015.

[78] Andres Macho, Maria Morant, and Roberto Llorente, "Next-Generation Optical Fronthaul Systems Using Multicore Fiber Media," J. Lightwave Tech., vol. 34, no. 20, pp. 4819-4827, Oct. 2016.

[79] Maria Morant and Roberto Llorente, "Experimental Demonstration of LTE-A M×4×4 MIMO Radio-over-Multicore Fiber Fronthaul," in Proc. Opt. Fiber Commun. Conf. (OFC) 2017, Th4E.4.

[80] Yi Lei, Jianqiang Li, Yuting Fan, Ming Tang, Feifei Yin, Yitang Dai, Kun Xu, Yuefeng Ji, "Space-Division-Multiplexed Transmission of IEEE 802.11ac-Compliant 6×6 WLAN Signals over 2-km 7-core Fiber," Asia Communications and Photonics Conferene (ACP), 2016, AF1H.2.

[81] Maria Morant, Andres Macho and Roberto Llorente, "On the Suitability of Multicore Fiber for LTE–Advanced MIMO Optical Fronthaul Systems," J. Lightwave. Tech., vol. 34, no. 2, pp. 676-682, Jan. 2016.

[82] Qi Mo, Jiale He, Dawei Yu, Lei Deng, Songnian Fu, Ming Tang, And Deming Liu, "2×2 MIMO OFDM/OQAM radio signals over an elliptical core few-mode fiber," Opt. Lett., vol. 41, no. 19, pp-4546-4549, Oct. 2016.

[83] Junpeng Liang, Qi Mo, Songnian Fu, Ming Tang, P. Shum, and Deming Liu, "Design and fabrication of elliptical-core few-mode fiber for MIMO-less data transmission," Opt. Lett., vol. 41, no. 13, pp. 3358-3361, Jul. 2016.

[84] H. Shin and M. Z. Win, "MIMO diversity in the presence of double scattering," IEEE Tran. Inf. Theory, vol. 54, no.7, pp. 2976-2996, Jul. 2008.

[85] Nenad Bozinovic, Y. Yue, Y. Ren, M. Tur, P. Kristensen, H. Huang, A. E. Willner, S. Ramachandran, "Terabit-Scale Orbital Angular Momentum Mode Division Multiplexing in Fibers," Science, vol. 340, pp. 1545-1548, Jun. 2013.

[86] Reza Mirzaei Nejad, K. Allahverdyan, P. Vaity, S. Amiralizadeh, C. Brunet, Y. Messaddeq, S. LaRochelle, and L. A. Rusch, "Mode Division Multiplexing Using Orbital Angular Momentum Modes Over 1.4-km Ring Core Fiber," J. Lightwave Technol., vol. 34, no. 18, pp. 4252-4258, Sept. 2016.

[87] Ezra Ip, G. Milione, Ming-Jun Li, Neda Cvijetic, Konstantinos Ka-nonakis, Jeffery Stone, Gaozhu Peng, Xesús Prieto, Carlos Monte-ro, Vicente Moreno, and Jesús Liñares, "SDM transmission of re-al-time 10GbE traffic using commercial SFP + transceivers over 0.5km elliptical-core few-mode fiber," Optics Express, vol. 23, no. 13, pp. 17120-17126, Jun 2015.

[88] Joel Carpenter, B. C. Thomsen, and T. D. Wilkinson, "Degenerate Mode-Group Division Multiplexing," J. Lightw. Technol., vol. 30, no. 24, pp. 3946-3952, Dec. 2012.

[89] Lixian Wang, Reza Mirzaei Nejad, Alessandro Corsi, Jiachuan Lin, Younès Messaddeq, Leslie Rusch, Sophie LaRochelle, "Linearly polarized vector modes: enabling MIMO-free mode-division multiplexing", Optics Express, vol. 25, no.10, pp. 11736-11748, May 2017.

[90] Lixian Wang and Sophie LaRochelle, "Design of eight-mode polarization-maintaining few-mode fiber for multiple-input multiple-output-free spatial division multiplexing," Opt. Lett., vol. 40, no. 24, pp. Dec 2015.

[91] Tan Haifeng, Li Wei, Wang Tan, Fang Jian, Feng Zhiyong, "The Analysis on the Candidate Frequency Bands of Future Mobile Communication Systems," China Communications, Supplement no.1, pp. 140-149, 2015.

[92] Yi Lei, Jianqiang Li, Rui Wu, Yuting Fan, Songnian Fu, Feifei Yin, Yitang Dai, and Kun Xu, "Experimental study on the statistic characteristics of a 3x3 RF MIMO channel over a single conventional multimode fiber," Opt. Lett., vol. 42, no. 11, pp.2217-2220, Jun. 2017.